Single-ion anisotropy, crystal-field effects, spin reorientation transitions, and spin waves in R_2CuO_4 (R=Nd, Pr, and Sm)

Ravi Sachidanandam
School of Physics and Astronomy, Raymond and Beverly Sackler Faculty of Exact Sciences, Tel Aviv University, Tel Aviv 69978, Israel

T. Yildirim
University of Maryland, College Park, Maryland 20742
and National Institute of Standards and Technology, Gaithersburg, Maryland 20899

A. B. Harris
Department of Physics, University of Pennsylvania, Philadelphia, Pennsylvania 19104-6396

Amnon Aharony and O. Entin-Wohlman
School of Physics and Astronomy, Raymond and Beverly Sackler Faculty of Exact Sciences, Tel Aviv University, Tel Aviv 69978, Israel
(Received 5 February 1997)

We report a detailed study of single-ion anisotropy and crystal-field effects in rare-earth cuprates R_2CuO_4 (R=Nd, Pr, and Sm). It is found that most of the magnetic properties are mainly due to the coupling between the copper and rare-earth magnetic subsystem which exhibits a large single-ion anisotropy. This anisotropy prefers ordering of rare-earth moments along [100] for R=Pr and Nd and along [001] for R=Sm. Combined with a pseudodipolar interaction arising from the anisotropy of the R-Cu exchange, we can explain the magnetic structures of these materials. The spin reorientation transitions in Nd_2CuO_4 can be explained in terms of a competition between various interplanar interactions which arises because of the rapid temperature dependence of the Nd moment below about 100 K. Finally we introduce a simple two-dimensional model for the Nd spin-wave spectrum. For zero wave vector, this model gives two optical modes involving Cu spins whose temperature-dependent energies agree with experimental results and an acoustic mode whose energy is predicted to be of order $\sqrt{2k_4\Delta}\approx 5\mu$eV, where k_4 is the fourfold in-plane anisotropy constant and Δ is the Nd doublet splitting. [S0163-1829(97)04525-6]

I. INTRODUCTION

Magnetic interactions in rare-earth (R) cuprate R_2CuO_4 (RCO) systems have been the subject of extensive study[1–9] for various reasons. First and foremost the R cuprates (which become superconducting under electron doping) have a simpler structure than the hole-doped superconducting cuprates. In particular, R_2CuO_4 crystallizes in the tetragonal structure[2] known as the T' phase in which there are no apical O ions. Hence CuO sheets form a planar square lattice. However, it has been observed that for too small or too large rare-earth ions, the T' phase is not stable, as evident from the distorted structure of Gd_2CuO_4.[3,4] Pr_2CuO_4 (PCO) is at the limit of the T' phase: the next compound with a lighter R, La_2CuO_4 (LCO), crystallizes not in the T' phase, but instead in the more compressed T-phase, where the out-of-plane oxygens move to apical positions.[5] In this phase there is an orthorhombic distortion[10] which allows the existence of a weak Dzialoshinskii-Moriya interaction, which gives rise to weak ferromagnetism.[11] Besides the direct structural evidence from x-ray[4] and neutron diffraction,[6] the absence of weak ferromagnetism in the R_2CuO_4 system[4] with R=Nd, Pr, Sm, etc. is clear evidence for the absence of any distortion away from tetragonal symmetry. Second, rare-earth cuprates exhibit novel magnetic properties involving both the Cu and R subsystems. In the case of Ce-doped Sm_2CuO_4 (SCO), coexisting rare-earth magnetism and superconductivity has also been observed.[7] Therefore the nature of magnetic interactions which determine the three-dimensional (3D) magnetic structure and the correlation between rare-earth magnetism and superconductivity are both of fundamental importance.

We start by giving a brief overview of some of the magnetic properties of the RCO systems. An extensive study of neutron, specific heat, magnetization measurements, Raman, and many more experiments have led to the following conclusions. First of all, many magnetic properties of the Cu subsystem in RCO are the same as those in LCO.[8] In particular, one has (1) very strong Cu-Cu exchange in the CuO plane, and (2) very small Cu-Cu interplane exchange interactions. As a consequence (3) the antiferromagnetic (AFM) long-range ordering of Cu spins is characteristic of a 2D Heisenberg antiferromagnet with weak anisotropies and interplanar couplings which lead to a Néel temperature, T_N, in the range 250–320 K.[9] The fact that these features remain the same in the RCO family indicates that the presence of the R subsystem does not significantly modify the properties of the Cu subsystem. For example, the anisotropy of the spin-1/2 Cu subsystem can obviously not be attributed to a single-ion mechanism. Theoretical efforts, culminating in the work of Refs. 12 and 13 have shown that this anisotropy can be understood as arising from a small anisotropy in the exchange tensor due to a mechanism involving the combined

effects of Coulomb exchange and spin-orbit coupling. We assume that the CuO planes are not very different in *R*CO than in the tetragonal cuprate $Sr_2CuCl_2O_2$ (SCCO) which has no *R* ions, so that the anisotropy of the Cu-Cu exchange is the same in the *R*CO systems as in SCCO.[14,15]

However, there are several important differences in the magnetism and 3D spin structure of rare-earth cuprates and other cuprates without a magnetic rare-earth ion, such as LCO,[8] and SCCO.[14,15] Among these differences are the following. (1) Although it is now understood that the *R* ions exhibit magnetic moments that are mainly induced by the exchange field of the Cu ions,[6] the role of the *R*-*R* interactions is less well quantified. (2) Unlike LCO and SCCO, in *R*CO the Cu spins prefer a noncollinear arrangement[16] (which we will describe in detail below). Although it seems clear that this noncollinear structure is due to the presence of the *R* ions, the detailed analysis of the energetics of these noncollinear structures on the basis of a microscopic model has not yet been given. (3) In particular, the sequence of spin reorientation phase transitions in Nd_2CuO_4 (NCO)[6] (and the absence of such reorientations in PCO) has not been explained in terms of a microscopic model. (4) The spin-wave spectrum observed in NCO (Refs. 17–19) has not yet been obtained from a microscopic model which is consistent with the lowest temperature spin structure and which also correctly accounts for the temperature dependence of the Cu modes at zero wave vector.

There have been several theoretical efforts to understand these properties. An attempt to explain some of these magnetic properties is that of Yablonsky.[20] He developed a theory for the magnetic structure of NCO based on the symmetry of the system. He concluded that the noncollinear spin structure was stabilized by biquadratic interactions. Recently some of the present authors have developed a theory[21] in which the various anisotropic magnetic interactions in the cuprates can be given a microscopic explanation. From these interactions it was possible to have a global understanding of the 3D spin structure of various layered magnetic systems but the magnetic structure of NCO remained unexplained. The spin-wave spectrum of NCO has been the object of several experimental[17–19] and one theoretical investigation.[22] As a result of these studies one has a reasonable qualitative understanding of the spectrum. However, as we will discuss, there are some inconsistencies in the calculation that should be removed in order to arrive at a coherent picture of the spin-wave spectrum and its relation to the magnetic structures of NCO. In summary, a detailed consistent microscopic explanation of the properties mentioned in the preceding paragraph does not yet exist. It is the purpose of the present paper to remedy this situation.

Now we summarize the general features of the microscopic interactions we will invoke in order to explain the magnetic properties and phases of NCO, PCO, and SCO. In Sec. III we present detailed calculations of the crystal-field states which verify previous work[23,24] which showed that NCO and PCO have an easy plane perpendicular to the tetragonal axis. The same approach provides a microscopic explanation for the observation[7] that for SCO the tetragonal axis is an easy axis. This is the first important result of the present paper. We also obtain a systematic treatment of the fourfold in-plane anisotropy due to the crystal field which favors alignment in the plane along[25] [100] for NCO and PCO and along [110] for SCO.

As mentioned above, we assume that the Cu-Cu interactions are similar to those in LCO or other cuprates. Next, one may consider the Nd-Cu interactions. It has been suggested[22] that the strongest interaction is a ferromagnetic interaction between the Cu ions and the two Nd ions which are its nearest neighbors along the tetragonal axis. In Sec. IV we discuss the experimental evidence which implies[26] that the dominant Cu-Nd interactions are instead those between nearest neighboring Nd and Cu planes. As we shall discuss, these interactions cannot be the usual isotropic exchange interactions, because in that case the exchange field on a Nd ion would vanish when summed over the neighboring plaquette of Cu ions. Accordingly, it is necessary to consider anisotropic interactions, such as dipolar interactions.[20] However, the dipolar interaction has the wrong algebraic sign to explain the low-temperature phase of NCO. In any event, the magnitude of the dipolar interaction is too small to be relevant in this context. For NCO it is therefore necessary to introduce a pseudodipolar interaction which results from the anisotropic component of the Nd-Cu exchange interaction.[21] The dominance of this interaction implies that a Cu plane together with the nearest-neighboring Nd planes are tightly coupled. We then explain the sequence of spin reorientations in NCO and the lack of such transitions in PCO in terms of smaller couplings between adjacent tightly bound units. Within these smaller couplings, we infer the existence of competing Nd-Nd, Nd-Cu, and Cu-Cu interactions. The rapid temperature dependence of the Nd moment has a crucial effect on this competition and, with a proper choice of parameters, can lead to spin reorientation transitions at the observed[6] temperatures. In addition, this result explains the absence of such transitions in PCO at atmospheric pressure. This explanation and the inferred dominance of the nearest-neighbor Cu-Nd interactions is the second important result of the present paper.

The final phenomenon which we address in Sec. V of this paper is the spin-wave spectrum of NCO. There are two new ingredients in NCO which are not present in, say, LCO. The first of these is the existence of low-energy excitations on the rare-earth sublattices. These excitations will give rise to nearly flat optical magnon modes, reminiscent of the analogous rare-earth excitations in the rare-earth iron garnets.[27] The second new feature of NCO is the noncollinearity of both the Cu and Nd moments.[16] Another interesting feature of this system is the existence of a Goldstone mode which reflects a symmetry of the dipolar interactions with respect to a suitable rotation of the moments in the easy plane. When the fourfold anisotropy which must occur in a tetragonal environment is taken into account, this mode will develop a small gap. Our model for the calculation of the spin-wave spectrum is somewhat similar to Thalmeier's[22] except that, as mentioned, we assume a different Cu-Nd interaction to be dominant than does Thalmeier. Also, because we wish to reproduce the interesting observed[17] temperature dependence of the optical spin-wave modes which involve the Cu spins, we introduce a simplified 2D model which includes both Nd and Cu spins, rather than assume a static Cu exchange field as Thalmeier does. Our treatment indicates the need for additional experiments to probe the very low-energy regions of

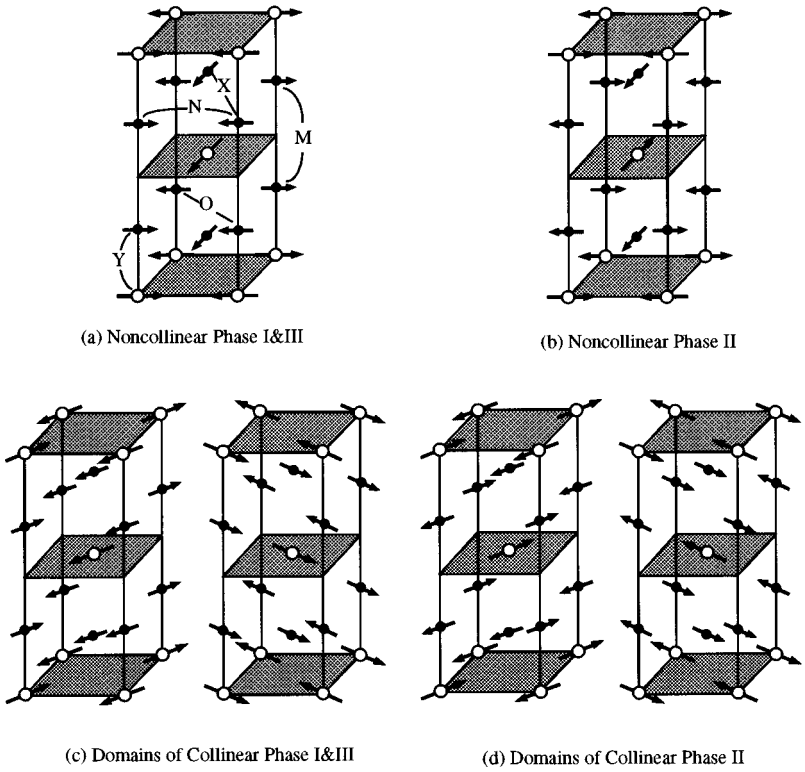

FIG. 1. Possible relative orientations of spins in the chemical unit cell of Nd_2CuO_4. Here the open circles are Cu ions and the filled ones *R* ions. Experiments in a magnetic field (Ref. 16) show that the actual structures are the noncollinear ones. We also indicate several of the interactions in our models for NCO.

the spin-wave spectrum to locate the Goldstone mode referred to above.

II. MAGNETIC STRUCTURE OF R_2CUO_4 (R=ND, PR, AND SM)

We summarize here various experimental results on the structure and properties of the *R*CO compounds which are relevant to our work. We first discuss the features common to all these materials. As the temperature is lowered, the 2D AFM correlations between Cu ions, which are well described by the 2D AFM Heisenberg model,[28] grow and, in the presence of even weak interplanar coupling, lead[9] to a phase transition at a temperature of order $T_N \approx 300$ K, below which there is long-range 3D AFM ordering. (The fact that the magnetic order in some *R*CO systems is noncollinear, rather than collinear as in LCO, is not expected to have a significant effect on T_N.) In contrast to materials like K_2MnF_4,[29] the magnetic anisotropy in the cuprates is such that the moments lie in the plane perpendicular to the tetragonal axis. In contrast to many materials where such anisotropy is explained in terms of single-ion anisotropy, here, because the Cu spin is 1/2, this anisotropy has been explained in terms of a Hubbard model in which the combined effect of Coulomb exchange and spin-orbit interactions lead to a small anisotropy in the exchange interactions between neighboring Cu ions.[30,12,13] In NCO we assume that as far as the Cu ions are concerned the picture for LCO remains intact. The fact that the interplanar couplings are stronger in NCO than in LCO will have only a small effect on the actual value of T_N. In tetragonal SCCO, a small in-plane anisotropy in which the [100] direction for the Cu moments is preferred over the [110] direction, has been predicted theoretically on the basis of zero-point spin-wave fluctuations,[21] and whose existence has been inferred from experiment in a related material.[31] As we shall see, such an in-plane anisotropy arises naturally in NCO from the much larger single-ion anisotropy of the Nd ion in the crystal electric field of its neighboring ions, as suggested by Yablonsky.[20] (For SCO the single-ion mechanism may not be dominant, as we discuss in Sec. III.) In the ordered phase the Cu magnetization, i.e., the thermally averaged value of the Cu spin, $\langle S \rangle_T$, of all the cuprates is the same and can be represented as[14,6,32–34]

$$\langle S \rangle_T = B(1 - T/T_N)^{\beta}. \tag{1}$$

For many cuprates $\beta \approx 0.25$.[32,35,36] To reproduce $\langle S \rangle_T$ over the entire temperature range for NCO we set $\beta = 0.3$ (Ref. 33) and take $B = 0.4$.

Next we discuss the noncollinear order found in the *R*CO's. In Fig. 1 we show two forms of noncollinear order and their collinearly ordered counterparts for NCO. In zero magnetic field the diffraction spectrum of a noncollinear structure is identical to that from a sample with equal populations of domains of the two corresponding collinear structures.[37] This fact caused some confusion which was resolved when the application of a symmetry-breaking magnetic field[16,33] showed that the noncollinear structures were the correct ones for NCO. Apart from field-dependent neutron-diffraction experiments, the strongest evidence for the noncollinear spin structure comes from the single-crystal magnetization experiment of Cherny *et al.*[38] They interpreted their data as showing a first-order phase transition for a field *H* applied along a [100] direction and a second-order phase transition for *H* applied along a [110] direction, indicating that the easy axis of the magnetization for Cu moments is [100] in the NCO system. We now summarize the experi-

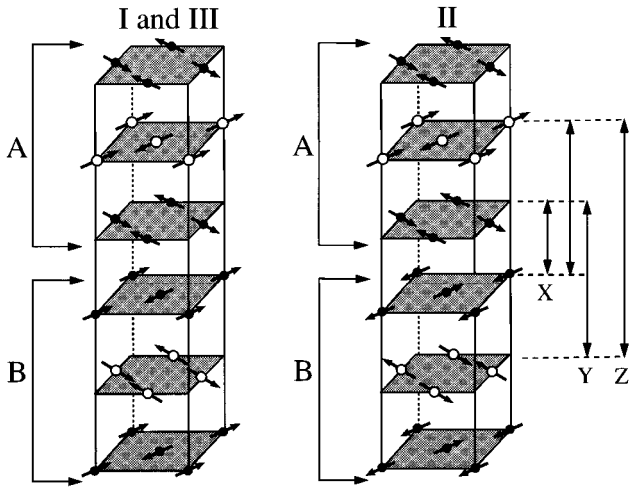

FIG. 2. The magnetic unit cell for the magnetically ordered phases I, II, and III of NCO. Note that the magnetic unit cell is twice as large as the chemical unit cell shown in Fig. 1. Also note that the [100] directions of the chemical unit cell are the diagonals of the square plaquettes shown here. The open circles are Cu ions and the filled ones R ions. Note that in all phases each set of three planes (one Cu plane together with its two neighboring Nd planes) forms a rigid unit (here labeled A and B) within which the relative spin orientations remain fixed. In passing from one phase to another the relative orientations of one rigid unit with respect to its neighboring rigid unit is reversed. At the far right we indicate the interaction energies X, Y, and Z, associated with interactions between spins in adjacent sets of planes. In each case, the interactions are those between nearest neighbors of the type in question.

ments which bear on the magnetic structure and single-ion properties of these RCO systems.

A. NCO

As the temperature is reduced, at $T_N \approx 255$ K the Cu moments order in the noncollinear structure of Fig. 1(a) (phase I), at $T_> = 75$ K the Cu spins reorder with the noncollinear structure of Fig. 1(b) (phase II), and at $T_< = 30$ K the Cu spins undergo another reorientation back to phase III which has the same noncollinear order as phase I, the high-temperature phase.[32,16,39] Below 2 K, there is evidence for two more transitions.[40] The transition at $T \approx 1.5$ K is attributed to ordering of Nd spins due to the Nd-Nd exchange interactions and the one at 0.5 K has been attributed to ''hyperfine-induced nuclear polarization'' by Chattopadhyay and Siemensmeyer.[41] Nd moments have also been observed below T_N, but above 1.5 K, which are supposed to be due to the exchange interaction with the Cu moments. At 0.4 K the Nd moment has been measured to be $1.3\mu_B$.[6]

In phases I and III the Cu and Nd moments along the z axis are parallel, while in phase II they are antiparallel.[42,43] This implies, as shown in Fig. 2, that the relative orientations of the Cu spins within one plane and the Nd spins in the nearest-neighboring planes above and below this Cu plane are fixed and do not change in going from one phase to another.

A systematic investigation of the crystal-field levels of the Nd ion using inelastic neutron scattering has been performed[24] and the results have been interpreted in terms of a crystalline electric-field model. In the presence of the exchange field from the Cu and Nd ions, the lowest doublet of the Nd ions has a splitting in energy, $\Delta \approx 0.32$ meV in the $T = 0$ limit, as determined by specific-heat measurements.[4] Raman experiments[44] give $\Delta = 0.35$ meV at $T = 20$ K and inelastic neutron-scattering measurements[45] give $\Delta = 0.35$ meV.

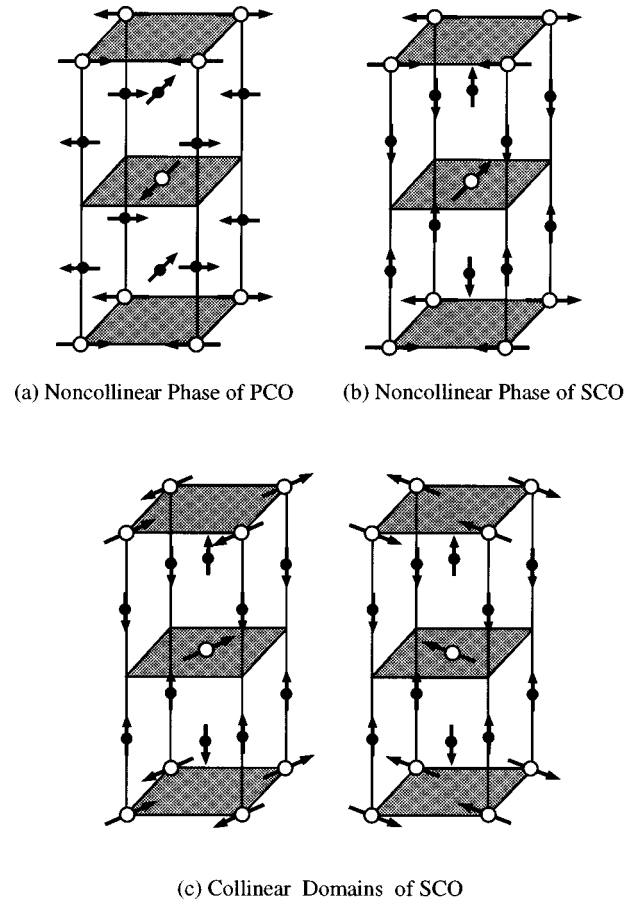

FIG. 3. As in Fig. 1. (a) The magnetic structure of PCO. (b) The noncollinear structure attributed (Refs. 34,47) to SCO for $T < 6$ K. We also show in (c) the corresponding collinear structures, since the existing data does not completely exclude them.

B. PCO

Long-range order of the Cu spins develops below $T_N \approx 285$ K, with an induced Pr ordering observed at lower temperatures. The Cu spin structure is a simple antiferromagnet in the a-b plane and (according to the neutron-scattering experiment with applied field **H** along the [100] direction) is noncollinear with the moments alternating along the [100] and [010] directions as one moves along the c axis as shown in Fig. 3(a).[33] The ordered moments for the Cu and Pr spins at about 10 K are 0.4 and 0.08 μ_B, respectively.[6] As the temperature is lowered no further transitions have been observed in this system. However, under pressure of 0.25 GPa, PCO behaves like NCO in having two spin reorientation transitions.[46] At atmospheric pressure a nearest-neighbor exchange constant $J = (130 \pm 30)$ meV and a spin-wave gap of

~ 5 meV was observed, which correspond to the reduced anisotropy constant $\alpha=(J-J_{xy})/J\sim 2\times 10^{-4}$. A systematic investigation of the crystal-field levels of the Pr ion using inelastic neutron scattering has been performed[23,24] and the results have been interpreted in terms of a crystalline electric-field model.

C. SCO

SCO differs significantly from NCO and PCO in several of its magnetic properties. As the temperature is reduced through $T_N\approx 280$ K, the Cu moments order in a structure with nonzero $[\frac{1}{2}\frac{1}{2}0]$ neutron Bragg intensity, implying existence of either the noncollinear structure of Fig. 1(b) or its collinear counterparts as shown in Fig. 1(d).[34,47] Neutron-scattering experiments[34,47] with an applied field along a [110] direction indicate no hysteresis above 20 K, which is consistent with the noncollinear spin structure shown in Fig. 1(b) and exclude the possibility of collinear ordering. However, below 20 K, unlike for NCO and PCO, strong hysteresis effects were observed. Such effects are not expected for noncollinear spin ordering (but are for collinear ordering). The definitive determination of the spin structure in SCO has to wait for a magnetization or neutron-scattering experiment with an applied field along a [100] direction. Such experiments were performed for NCO and unambiguously demonstrated the noncollinear spin structure of NCO.[38,16]

The second major difference between SCO and other *R* cuprates is the magnetic ordering of the *R* ions. Above about 10 K, unlike NCO or PCO, no evidence was found for any magnetic moment associated with Sm ions. In fact, our calculations predict this moment to be much smaller than in NCO or PCO. So, although in principle this induced Sm moment *must* exist, it is apparently too small to be observed up to now. However, below 6 K Sm ions exhibit long-range ordering with a spin structure totally different than that of NCO and PCO, as shown in Fig. 3(b). The Sm magnetic structure consists of ferromagnetic sheets within the *a*-*b* planes, with the spins in alternate sheets along the *c* axis aligned antiparallel to one another.[7] In this phase it is not established whether the structure is the noncollinear one shown in Fig. 3(b) or the collinear one shown in Fig. 3(c). The value of Sm moment at about 2 K was measured to be $0.37\mu_B$. As the temperature is lowered, another transition of a continuous nature below 1 K was observed. As mentioned, a very similar transition was also observed in NCO and was attributed to nuclear polarization of the *R* ions.[41]

III. RARE EARTHS IN *R*CO

We now calculate the magnetic response of R^{+3}-ions subject to tetragonal crystalline fields and a molecular field generated by the copper spins. Except at temperatures below about 10 K, one may neglect the *R*-*R* interactions and their contribution to the molecular field at a *R* site. Here we calculate the thermodynamic properties of the *R* subsystem at temperatures above, say, 10 K. This calculation will explain the easy axis of the *R* magnetization in *R*CO. We will treat the Cu-*R* interaction within the mean-field approximation. Therefore the Hamiltonian for the rare-earth ion in the presence of an exchange field **h** is

$$\mathcal{H}=\mathcal{H}_{\rm CEF}-\mathbf{J}\cdot\mathbf{h}\equiv\mathcal{H}_{\rm CEF}+V_{\rm ex}, \tag{2}$$

where $\mathcal{H}_{\rm CEF}$ is the crystal electric-field (CEF) potential and $V_{\rm ex}$ is the perturbation due to the exchange field. Our aim here is not to obtain a complete fit of all spectroscopically determined crystal-field energy levels, but rather to explain the anisotropy of the *R* ions. Accordingly we restrict our treatment to states in the lowest **J** multiplet. Within this multiplet vectors are proportional to **J** according to the Wigner-Eckart theorem.[48] Accordingly, we arbitrarily define the exchange field so that it couples to **J** and has the dimensions of energy.

A. Crystalline electric-field Hamiltonian $\mathcal{H}_{\rm CEF}$

The crystal electric-field Hamiltonian $\mathcal{H}_{\rm CEF}$, constructed to be the most general one consistent with the *R*-site symmetry, D_4, is

$$\mathcal{H}_{\rm CEF}=\sum_{k=2,4,6}\sum_{m=-k}^{k}A_k^{|m|}\left(\frac{4\pi}{2k+1}\right)^{1/2}\sum_{i=1}^{3}\langle r_i^k Y_k^m(\Omega_i)\rangle, \tag{3}$$

where the sum over i is over the three electrons in the unfilled $4f$ shell and the sum over k is restricted to 2, 4, and 6 because only these values of k have nonzero matrix elements within the manifold of $l=3$ states of the $4f$ shell. In the sum over m only terms for which $|m|/4$ is an integer or zero are nonzero, as a result of the fourfold axis of rotation about the z axis at the *R* site. The factors A_k^m are approximately the same for different rare earths in a given environment. It has been shown by Stevens[49] that when we restrict attention to a manifold of states corresponding to a single value of J, then this potential can be rewritten in terms of the **J** operators. In this case,

$$\mathcal{H}_{\rm CEF}=B_2^0O_2^0+B_4^0O_4^0+B_4^4O_4^4+B_6^0O_6^0+B_6^4O_6^4, \tag{4}$$

where the Stevens operators O_k^m are

$$O_2^0=3J_z^2-J(J+1),$$

$$O_4^0=35J_z^4-30J(J+1)J_z^2+25J_z^2-6J(J+1)+3J^2(J+1)^2,$$

$$O_4^4=\frac{1}{2}(J_+^4+J_-^4),$$

$$\begin{aligned}O_6^0=&231J_z^6-315J(J+1)J_z^4+735J_z^4+105J^2(J+1)^2J_z^2\\&-525J(J+1)J_z^2+294J_z^2,\\&-5J^3(J+1)^3+40J^2(J+1)^2-60J(J+1),\end{aligned}$$

$$\begin{aligned}O_6^4=&\frac{1}{4}\{[11J_z^2-J(J+1)-38(J_+^4+J_-^4)\\&+(J_+^4+J_-^4)(11J_z^2-J(J+1)-38]\},\end{aligned} \tag{5}$$

and B_k^m are the CEF parameters

$$B_k^m=A_k^m\langle r^k\rangle\alpha_k/\beta_k^m, \tag{6}$$

where $\langle r^k\rangle$ is the average of r^k taken over a $4f$ radial wave function,[50] the factor α_k is the Stevens coefficient,[49] and

TABLE I. The crystal-field parameters B_k^m of Eq. (4) (in μeV) for R^{3+} in RCO.

B_k^m	Nd	Pr	Sm
B_2^0	128	170	−841.7
B_4^0	10	23	−59.1
B_4^4	−62	−170	−539.0
B_6^0	−0.064	0.05	
B_6^4	−4.877	7.4	

β_k^m is given by Kassman.[51] In Table I we list the values of the B coefficients we obtained from various experimental works[24,52] and which we have used for our simplified (in that we treat only the ground J multiplet) calculations. We have verified that the corresponding values of A_k^m obtained using Eq. (6) do not vary greatly from one R ion in RCO to the next. One sees this from Table II where we list the values of $A_k^m\langle r^k\rangle$. (The values of $\langle r^k\rangle$ are the same within a factor of 2 from one R ion to the next.[50])

B. Crystal-field levels

The ground-state J multiplet of any rare-earth ion, R^{3+}, is specified by Hund's rules.[53] The splitting of the $2J+1$-fold degenerate ground state in the tetragonal crystalline environment of the various compounds can be qualitatively studied using group theory.[54] For quantitative results the potential of Eq. (4) is diagonalized to get the eigenstates. For our study of the rare-earth anisotropy, we confine our attention to the lowest J multiplet. Accordingly, $|M\rangle$ will denote the wave function $|J,M\rangle$, where the value of J is implicit. Since one expects that the tetragonal symmetry crystalline electric field is not extremely different from what one would have under cubic symmetry, we will show how the energy-level scheme compares to the cubic symmetry results of Lea *et al.* (LLW).[55] In the present case, the cubic CEF Hamiltonian, $\mathcal{H}_{\rm cub}$, assumes the form

$$\mathcal{H}_{\rm cub}=\frac{Wx}{F(4)}(O_4^0-5O_4^4)+\frac{W(1-|x|)}{F(6)}(O_6^0+21O_6^4), \quad (7)$$

where $F(4)=60$ and $F(6)$ assumes the values 2520 and 1260 for Nd and Pr, respectively, and is irrelevant for Sm. The noncubic tetragonal components, $\mathcal{H}_{\rm tet}$, are fixed by the condition $\mathrm{Tr}\mathcal{H}_{\rm cub}\mathcal{H}_{\rm tet}=0$ to be $O_4^0+7O_4^4$ and $O_6^0-3O_6^4$. Any tetragonal CEF is thus a unique linear combination of a cubic and a noncubic tetragonal CEF.

TABLE II. The crystal-field parameters $A_k^m\langle r^k\rangle$ in meV for R^{3+} in RCO.

	Nd	Pr	Sm
$A_2^0\langle r^2\rangle$	−40	−16	−40.8
$A_4^0\langle r^4\rangle$	−280	−251	−189
$A_4^4\langle r^4\rangle$	204	221	206
$A_6^0\langle r^6\rangle$	27	13	
$A_6^4\langle r^6\rangle$	183	173	

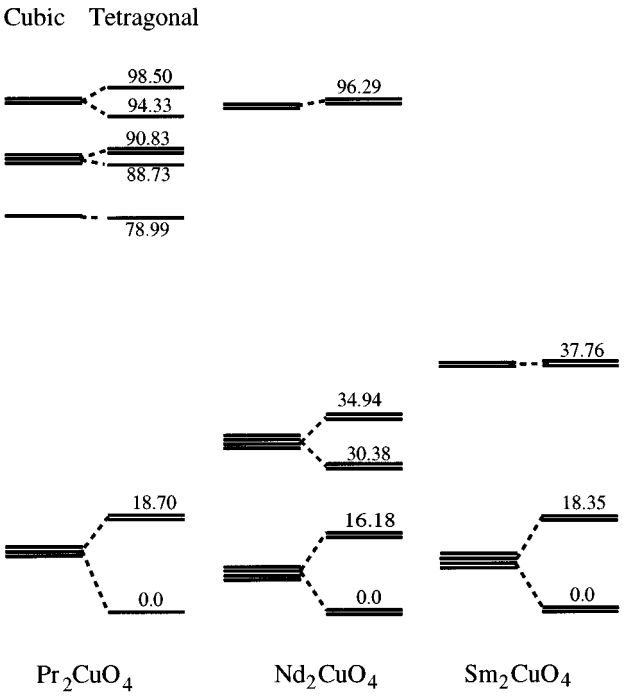

FIG. 4. Schematic diagrams of the CEF energy levels and states of PCO (left panel), NCO (middle panel), and SCO (right panel) in the cubic and tetragonal crystalline-electric field (CEF). Our approximate calculations agree qualitatively with more accurate calculations including all multiplets (Ref. 24).

1. Nd^{+3} $^4I_{9/2}$ ($S=3/2$, $L=6$, ground multiplet $J=9/2$, $g_J=8/11$)

Group theory tells us that in view of the Kramers degeneracy the tenfold degenerate ground multiplet will split into five doublets. Diagonalizing the CEF Hamiltonian, we find the five doublets, whose wave functions (in order of increasing energy) are

$$|A_1\rangle=0.482|9/2\rangle+0.638|1/2\rangle+0.601|-7/2\rangle, \quad (8a)$$

$$|A_2\rangle=0.971|5/2\rangle-0.237|-3/2\rangle, \quad (8b)$$

$$|A_3\rangle=0.543|9/2\rangle+0.321|1/2\rangle-0.776|-7/2\rangle, \quad (8c)$$

$$|A_4\rangle=0.237|5/2\rangle+0.971|-3/2\rangle, \quad (8d)$$

$$|A_5\rangle=0.688|9/2\rangle-0.700|1/2\rangle+0.192|-7/2\rangle. \quad (8e)$$

We have given only one of the partners in each doublet. The corresponding energies are shown in Fig. 4, where for comparison we also show the levels scheme when only the cubic component of the CEF is retained, where we have $x=-0.554$ and $W=-1.192$ meV.

Since we will be carrying out perturbative and numerical treatments of the effect of the exchange field on these states, we now discuss them briefly. Using the fact that the time-reversal operator, Θ, acting on an angular momentum eigenstate results in

$$\Theta|J,M\rangle=(-1)^{J-M}|J,-M\rangle, \quad (9)$$

we find the partner of $|A_i\rangle$ in the ith doublet, denoted $|B_i\rangle$, to be

$$|B_i\rangle = (-1)^{2J}\Theta^2|B_i\rangle = \Theta|A_i\rangle. \quad (10)$$

Naturally, $\langle B_i|A_i\rangle = 0$. Note that even though the doublet is degenerate, we may specify the doublet wave functions uniquely to within a phase factor by requiring that rotation about the z axis by $\pi/2$ gives back the original wave function with at most an added phase. Note that $|A\rangle$ and $|B\rangle$ satisfy this requirement but nontrivial linear combinations of them do not.

2. Pr^{+3} $^3H_4$ ($S=1$, $L=5$, ground multiplet $J=4$, $g_J=4/5$)

Group theory tells us that the ninefold degenerate ground multiplet will split into two doublets ($|D_i\rangle$ and $|d_i\rangle$) and five singlets. We find the eigenstates (in order of increasing energy) to be

$$|g\rangle \equiv |e_0\rangle = 0.707|2\rangle + 0.707|-2\rangle, \quad (11a)$$

$$|d_1\rangle = 0.876|3\rangle + 0.483|-1\rangle, \quad (11b)$$

$$|e_1\rangle = -0.427|4\rangle + 0.797|0\rangle - 0.427|-4\rangle, \quad (11c)$$

$$|e_2\rangle = 0.707|4\rangle - 0.707|-4\rangle, \quad (11d)$$

$$|D_1\rangle = -0.483|3\rangle + 0.876|-1\rangle, \quad (11e)$$

$$|e_3\rangle = 0.564|4\rangle + 0.604|0\rangle + 0.564|-4\rangle, \quad (11f)$$

$$|e_4\rangle = -0.707|2\rangle + 0.707|-2\rangle. \quad (11g)$$

The doublet partners are $|d_2\rangle = \Theta|d_1\rangle$ and $|D_2\rangle = \Theta|D_1\rangle$. Here when the noncubic contributions to the CEF are neglected one has the LLW parameters $x = 0.807$ and $W = 2.051$ meV. The eigenenergies are shown in Fig. 4 and they agree with the observed energies to within an error of 20%. This error can be reduced if we include admixtures of the higher J multiplets.[24]

3. Sm^{+3} $^6H_{5/2}$ ($S=5/2$, $L=5$, ground multiplet $J=5/2$, $g_J=6/7$)

Group theory tells us that in view of the Kramers degeneracy the sixfold degenerate ground J multiplet will split into three doublets. We find the eigenstates (in order of increasing energy) to be

$$|A_1\rangle = 0.906|5/2\rangle - 0.423|-3/2\rangle, \quad (12a)$$

$$|A_2\rangle = |1/2\rangle, \quad (12b)$$

$$|A_3\rangle = 0.423|5/2\rangle + 0.906|-3/2\rangle, \quad (12c)$$

with the partners in the doublet given by $|B_i\rangle = \Theta|A_i\rangle$. The corresponding energies are shown in Fig. 4. When the noncubic components of the CEF are neglected, we have the LLW parameters $W = -4.763$ meV and $x = 1.0$. It is also important to note that the lowest excited multiplet $J = 7/2$ lies at about 150 meV above the ground state,[52] compared to 270 meV for NCO (Ref. 56) and 300 meV for PCO.[57] Hence, of all our results, those for SCO are the most likely to suffer from not including J-mixing effects.

C. Effect of an exchange field on the rare-earth ion

1. Energy levels in the exchange field

We start by discussing the calculation of the energy levels when the exchange interaction, V_{ex} of Eq. (2), is treated perturbatively. For the present it is not important which Cu ion is responsible for this interaction. As we shall see, we will need to obtain the energy levels correctly up to order h^4.

First we discuss the calculations for NCO. (The calculations for SCO, which is also a Kramer's ion, were done analogously.) We consider the energies of the 10 levels of the $J = 9/2$ state in a D_4 CEF and a weak exchange field, h, as expansions in powers of h. Thus we write

$$E_i(\mathbf{h}) = E_i(0) + E_{i1} + E_{i2} + E_{i3} + E_{i4} + \ldots \equiv E_i(0) + E_i', \quad (13)$$

where E_{in} is the nth order (in h) correction to the $E_i(h=0)$ energy due to the exchange field. To develop the perturbation series, we note that the states are doubly degenerate. To implement perturbation theory we must first diagonalize the perturbation matrix V_{ex} within the doublet states. Then these eigenstates are used to perform the rest of the perturbation calculation. We now evaluate the matrix elements of the potential between the various states. We start with the relation

$$\Theta \mathbf{J} \Theta = -\mathbf{J}, \quad (14)$$

where Θ is the time-reversal operator. This along with Eq. (10) gives us

$$\langle A_k|J^+|B_l\rangle = \langle A_k|\Theta\Theta J^+ \Theta\Theta|B_l\rangle = \langle A_l|J^-|B_k\rangle, \quad (15)$$

where $J^{\pm}$ are the usual raising and lowering operators. From the form of the wave functions and the relation above we have

$$\begin{pmatrix} \langle A_k| \\ \langle B_k| \end{pmatrix} J^+(|A_l\rangle|B_l\rangle) = x_{kl}(\sigma_x + i\epsilon_{kl}\sigma_y), \quad (16a)$$

$$\begin{pmatrix} \langle A_k| \\ \langle B_k| \end{pmatrix} J^-(|A_l\rangle|B_l\rangle) = x_{kl}(\sigma_x - i\epsilon_{kl}\sigma_y), \quad (16b)$$

$$\begin{pmatrix} \langle A_k| \\ \langle B_k| \end{pmatrix} J_z(|A_l\rangle|B_l\rangle) = z_{kl}\sigma_z, \quad (16c)$$

where $|A_k\rangle, |B_k\rangle$ are the two members of the kth doublet, defined in Eqs. (8) and (10), σ are the Pauli matrices, and ϵ_{ij} is given by

$$\epsilon_{ij} = (-1)^{i+j}. \quad (17)$$

In Tables III and IV we list the values of the symmetric matrices x_{kl} and z_{kl} for NCO which we calculated from the CEF eigenstates of Eqs. (8). Tables V and VI contain the analogous results for SCO based on Eqs. (12).

To get the zeroth-order wave function and the first-order corrections to the energies we diagonalize

$$\begin{pmatrix} \langle A_k| \\ \langle B_k| \end{pmatrix} V_{ex}(|A_k\rangle|B_k\rangle) = \begin{pmatrix} z_{kk}h_z & x_{kk}h_\perp e^{-i\phi} \\ x_{kk}h_\perp e^{i\phi} & -z_{kk}h_z \end{pmatrix}, \quad (18)$$

TABLE III. The x_{kl} matrix for Nd in NCO.

	1	2	3	4	5
1	1.886	0.796	0.444	1.803	−0.358
2	0.796	−1.056	−1.694	2.033	0.780
3	0.444	−1.694	−1.008	0.395	−1.205
4	1.803	2.033	0.395	1.056	−1.575
5	−0.358	0.780	−1.205	−1.575	1.622

where z_{kk} and x_{kk} are defined in Eqs. (16), $h_\perp$ is the component of magnetic field perpendicular to the z axis, and ϕ is the angle between this component and the x axis. We denote the zeroth-order eigenstates of $V_{\rm ex}$ by $|k+,0\rangle$ and $|k-,0\rangle$. Under Θ we have

$$|k+,0\rangle = -\Theta^2|k+,0\rangle = \Theta|k-,0\rangle. \tag{19}$$

Using these, with $\Theta V_{\rm ex}\Theta = -V_{\rm ex}$, we get

$$E_{k_+1} = \langle k+,0|V_{\rm ex}|k+,0\rangle = -E_{k_-1}, \tag{20}$$

where $E_{k_\pm 1}$ is the first order correction to the energy of the eigenstate $|k\pm,0\rangle$. Similarly,

$$E_{k_+n} = E_{k_-n}, \quad \text{for even } n \tag{21a}$$

$$E_{k_+n} = -E_{k_-n}, \quad \text{for odd } n. \tag{21b}$$

We can calculate the various terms that appear in the expansion to fourth order in the perturbation theory to obtain

$$E_{i_+1} = \lambda_i = \sqrt{x_{ii}^2 h_\perp^2 + z_{ii}^2 h_z^2}, \tag{22a}$$

$$E_{i_+2} = a_{2i}h_\perp^2 + b_{2i}h_z^2, \tag{22b}$$

$$E_{i_+3} = [a_{3i}(h_x^4 + h_y^4) + b_{3i}h_x^2h_y^2 + c_{3i}h_z^2h_\perp^2 + d_{3i}h_z^4]/\lambda_i, \tag{22c}$$

$$E_{i_+4} = a_{4i}(h_x^4 + h_y^4) + b_{4i}h_x^2h_y^2 + c_{4i}h_z^2h_\perp^2 + d_{4i}h_z^4, \tag{22d}$$

where $h_\perp^2 = h_x^2 + h_y^2$. Analytic expressions for the coefficients are given in Appendix A and their numerical values are listed in Table VII for NCO and in Table VIII for SCO. Keeping in mind that the third-order terms are more important than the fourth-order terms (these are relevant only in the high-temperature expansion of the free energy), we can see from the fact that $2a_{3,1} - b_{3,1}$ is positive that the energy of the ground state is minimized when the exchange field is along the [100] or [010] directions. Let $h_z = 0$. Then it is easy to see that the energy of the ground state (or any state for that matter) has a linear dependence on the field, and hence it has a component of **J** along the exchange field given by x_{11}. The higher-order terms give the induced contribution to **J** due to the exchange field. The analogous results for the ground state of Pr (which is not a Kramer's ion) are discussed in Appendix C.

TABLE IV. The z_{kl} matrix for Nd in NCO.

	1	2	3	4	5
1	−0.015	0.000	2.911	0.000	0.864
2	0.000	2.275	0.000	0.922	0.000
3	2.911	0.000	−0.729	0.000	2.090
4	0.000	0.922	0.000	−1.275	0.000
4	0.864	0.000	2.090	0.000	2.244

TABLE V. The x_{kl} matrix for Sm in SCO.

	1	2	3
1	−0.857	−0.598	0.718
2	−0.598	1.500	1.281
3	0.718	1.281	0.857

2. Susceptibilities and in-plane anisotropy

Having the perturbation expansion for each energy level we can easily obtain expansions in powers of **h** for the partition function, $Z \equiv \Sigma_i \exp(-\beta E_i)$ and then the free energy, $F \equiv -kT\ln Z$. For tetragonal symmetry this expansion takes the form (up to order h^4)

$$F(h) = F(0) - \frac{1}{2g_J^2}\chi_\parallel h_z^2 - \frac{1}{2g_J^2}\chi_\perp h_\perp^2 + \alpha_4(h_x^4 + h_y^4) + \beta_4 h_z^4 + \gamma_4 h_x^2 h_y^2 + \delta_4 h_\perp^2 h_z^2, \tag{23}$$

the coefficients are given in Appendix B in terms of the coefficients appearing in Eq. (22). The Landé g value appears here because the external field couples to $g_J\mathbf{J}$ rather than just to **J** [see Eq. (2)]. Incorporating the isotropic terms in $F_0(h^2)$, we may write

$$F(\mathbf{h}) = F_0(h^2) + \frac{1}{2g_J^2}(\chi_\perp - \chi_\parallel)\left(h_z^2 - \frac{1}{3}h^2\right) - K_4(h_x^4 + h_y^4 - 6h_x^2h_y^2) + \ldots, \tag{24}$$

which defines the fourth-order anisotropy constant, K_4, given by $K_4 = (\gamma_4 - 2\alpha_4)/8$. We have used the standard expressions (given in Appendix B for NCO and SCO and in Appendix C for PCO) to evaluate the susceptibilities for the systems under consideration, and the results are shown in Fig. 5.

Some comments on these results are in order. Note that our results for Nd and Pr are very similar to those of Boothroyd *et al.*[24] who took account of all J multiplets. Also it is interesting that at high temperature the anisotropy between $\chi_\perp$ and $\chi_\parallel$ (see Fig. 5) for Pr in PCO is much larger than for Nd in NCO. This is an unexpected result: one might have thought that Nd must have larger anisotropy, since it has a moment whereas Pr has a nonmagnetic ground state.

TABLE VI. The z_{kl} matrix for Sm in SCO.

	1	2	3
1	1.784	0.000	1.533
2	0.000	0.500	0.000
3	1.533	0.000	−0.784

TABLE VII. The coefficients in the energy expansion for the ith CEF doublet of Nd^{3+} in NCO. These coefficients are in units such that when the exchange field is in meV, they give the energy contribution in meV. Listed here are the values of $100a_2(i)$, etc.

	$i=1$	$i=2$	$i=3$	$i=4$	$i=5$
$10^2a_2(i)$	−14.1	−38.5	15.1	30.4	7.1
$10^2b_2(i)$	−28.8	−4.5	21.4	4.5	7.4
$10^3a_3(i)$	−2.1	−8.7	−51.0	−59.7	−1.9
$10^2b_3(i)$	−16.6	−2.5	17.0	−9.0	0.2
$10^2c_3(i)$	−1.8	−14.9	6.5	8.9	−1.0
$10^3d_3(i)$	0.0	−19.0	−3.2	−10.6	−3.4
$10^2a_4(i)$	0.0	1.05	−3.81	2.77	0.00
$10^2b_4(i)$	−1.27	2.87	1.88	−3.51	0.02
$10^3c_4(i)$	−4.0	13.1	−5.4	−3.8	0.0
$10^3d_4(i)$	2.10	−1.45	−2.14	1.45	0.04

However as we shall see below, the anisotropy within the plane for Nd is much larger than for Pr at temperatures below 150 K. The right panel of Fig. 5 shows the susceptibilities of Sm in SCO. Note that they are completely different from those of Pr and Nd. First of all, for Sm in SCO, $\chi_\parallel$ is larger than $\chi_\perp$. This indicates that Sm moments prefer to lie along the [001] direction. The second major difference concerns the magnitudes of $\chi_\parallel$ and $\chi_\perp$, which are both much smaller than in PCO or NCO. Thus it is not surprising that experiments[7] show that in SCO the Sm and Cu sublattices are nearly decoupled.

To analyze the anisotropy within the plane, it is necessary to study K_4. If $\chi_\parallel < \chi_\perp$, then the easy axis is a [100] direction if K_4 is positive and is a [110] direction if K_4 is negative. We should also note that the anisotropy at $T=0$ is easily deduced from the expansion for the ground-state energy given in Eq. (22). For SCO, we determine the easy direction of the Sm moments when they are constrained (as we might assume by their interactions with the Cu ions) to lie in the CuO plane. In Fig. 6 we show our calculations of K_4 for NCO and SCO done in two ways. At temperatures large compared to the doublet splitting, we evaluated $K_4=(\gamma_4-2\alpha_4)/8$ using the analytic expressions for these coefficients in Appendix B. We also carried out an approximate evaluation of K_4, by numerically calculating the free energy, $F_{100}(T)$ for **h** along [100] and $F_{110}(T)$ for **h** along [110] and associating $F_{110}(T)-F_{100}(T)$ with $2K_4h^4$.

TABLE VIII. The coefficients in the energy expansion for the ith CEF doublet of Sm^{3+} in SCO. These coefficients are in units such that when the field is in meV, they give the energy contribution in meV. The doublets are labeled in order of decreasing energy.

	$i=1$	$i=2$	$i=3$
$10^2a_2(i)$	−3.31	−6.50	9.82
$10^2b_2(i)$	−6.22	0.0000	6.22
$10^3a_3(i)$	−1.32	−3.33	0.06
$10^2b_3(i)$	0.83	−7.75	−4.36
$10^3c_3(i)$	−7.63	−3.89	5.22
$10^3d_3(i)$	−7.55	0.00000	−3.32
$10^4a_4(i)$	−1.05	3.81	−2.76
$10^3b_4(i)$	−0.06	−4.94	4.99
$10^3c_4(i)$	−0.79	1.63	−0.84
$10^4d_4(i)$	−1.85	0.000000	1.85

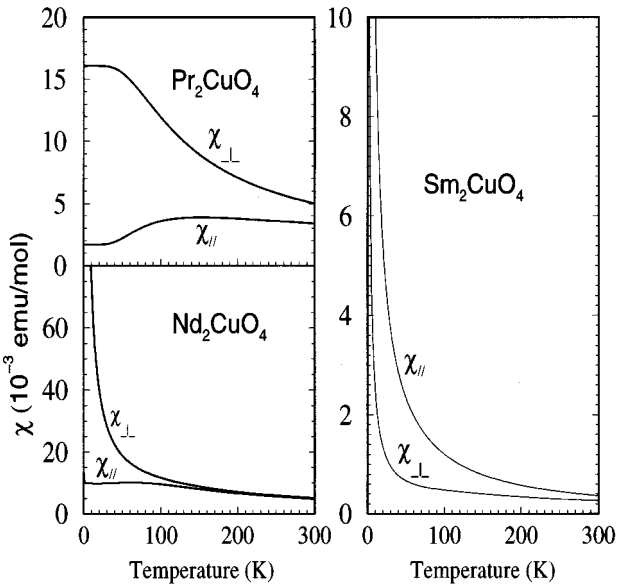

FIG. 5. Temperature dependence of the magnetic susceptibility parallel ($\chi_\parallel$) and perpendicular ($\chi_\perp$) to the tetragonal c axis for three RCO's. Note that the anisotropy (between $\chi_\perp$ and $\chi_\parallel$) for PCO is actually larger than for NCO at high temperature, which is an unexpected result. The right panel shows $\chi_\parallel$ and $\chi_\perp$ for SCO. Note that for SCO (unlike for NCO or PCO) $\chi_\perp$ is smaller than $\chi_\parallel$. Also the magnitude of the susceptibility of Sm is much smaller than that of Pr and Nd. Our calculations agree with those of Refs. 24 and 23 for PCO and of Ref. 24 for NCO.

The fact that for NCO K_4 is positive at all temperatures indicates that the Nd moments prefer the noncollinear struc-

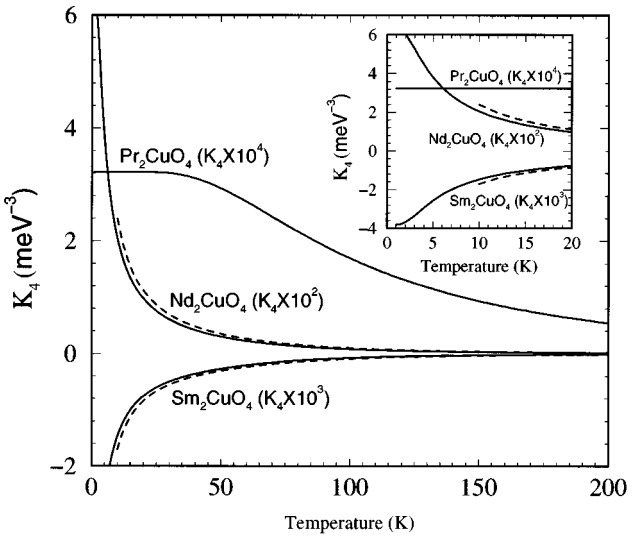

FIG. 6. The in-plane anisotropy $K_4(T)$ for NCO and SCO (full line) calculated numerically, as described in the text, compared to the perturbation result (dotted line) $K_4=(\gamma_4-2\alpha_4)/8$. For PCO we show only the numerical result. The zero-temperature result implied by Eq. (25) agrees perfectly with the numerical result. Note that K_4 is at least one order of magnitude larger for NCO than for SCO.

ture in which they are oriented along [100] directions. (This conclusion assumes that the exchange field acting on the Nd spins is a pseudodipolar one, so that as far as such interactions are concerned, the collinear and noncollinear structures would have the same energy, see discussion below.) For SCO one sees the reverse result. However, one still has to consider the contribution from the anisotropic Cu-Cu exchange interactions to the anisotropy within the plane. We study this effect in Appendix E for NCO and show that it is dominated by the intrinsic Nd anisotropy due to the CEF acting on the Nd ions. For SCO, where K_4 is at least an order of magnitude smaller, and where the value of **h** is not known, it is possible that the anisotropy due to the anisotropic Cu-Cu exchange could be dominant. Since this anisotropy favors orientation along [100], we cannot be certain which direction in the CuO plane is favored. Clearly this topic requires further theoretical and experimental investigation.

For PCO we only carried out the perturbative evaluation of K_4 at zero temperature, since for a non-Kramer's ion, the temperature dependences will be less pronounced. The calculation of the ground-state energy is simplified by the fact that only a few of the matrix elements of $V_{\rm ex}$ are nonzero. The details of the calculation are given in Appendix C and the final result is

$$E_g = -0.389h_\perp^2 - 0.040h_z^2 + 0.00696(h_x^4 + h_y^4) + 0.0165h_x^2h_y^2 + 1.674\times 10^{-5}h_z^4 - 0.00447h_\perp^2h_z^2, \quad (25)$$

where E_g and **h** are in meV. In the notation of Eq. (24) this result implies that $K_4(T=0) = \gamma_4/8 - \alpha_4/4 = 3.2\times 10^{-4}$ meV. From Eq. (25) we see that the terms of order h^2 lead to an easy plane and the fact that K_4 is positive indicates that [100] is an easy direction of magnetization. The numerical evaluation of K_4 (shown in Fig. 6) confirms that the essential results are not very different at nonzero temperature.

We would point out an interesting behavior of the two Pr doublets in the presence of the exchange field. Normally a doublet will show an energy splitting linear in h. Here, this happens if the field is oriented along the z axis. However, under normal conditions the exchange field is in the plane, in which case the splitting is proportional to h^2. In general, the splittings Δ_d and Δ_D between the two states of the doublets d_i and D_i, respectively, is given by

$$\Delta_a = 2(p_a h_z^2 + q_a h_\perp^4)^{1/2}, \quad (26)$$

with

$$p_a = \langle a_1|J_z|a_1\rangle^2, \quad q_a = \left| \sum_e \frac{\langle a_1\Theta|J_x|e\rangle\langle e|J_x|a_1\rangle}{E_a - E_e} \right|^2, \quad (27)$$

where $a=d$ or $a=D$ labels the doublet. Numerically we find $p_d = 4.28$, $p_D = 0.0046$, and in $(\text{meV})^{-2}$, $q_d = 0.031$, and $q_D = 0.25$.

3. The rare-earth magnetic moments

In this section we discuss the magnetic moments of Nd and Pr within the framework of the crystal-field approximation given in Eq. (2). In Fig. 7 we show the experimental results of the rare-earth magnetization versus temperature for

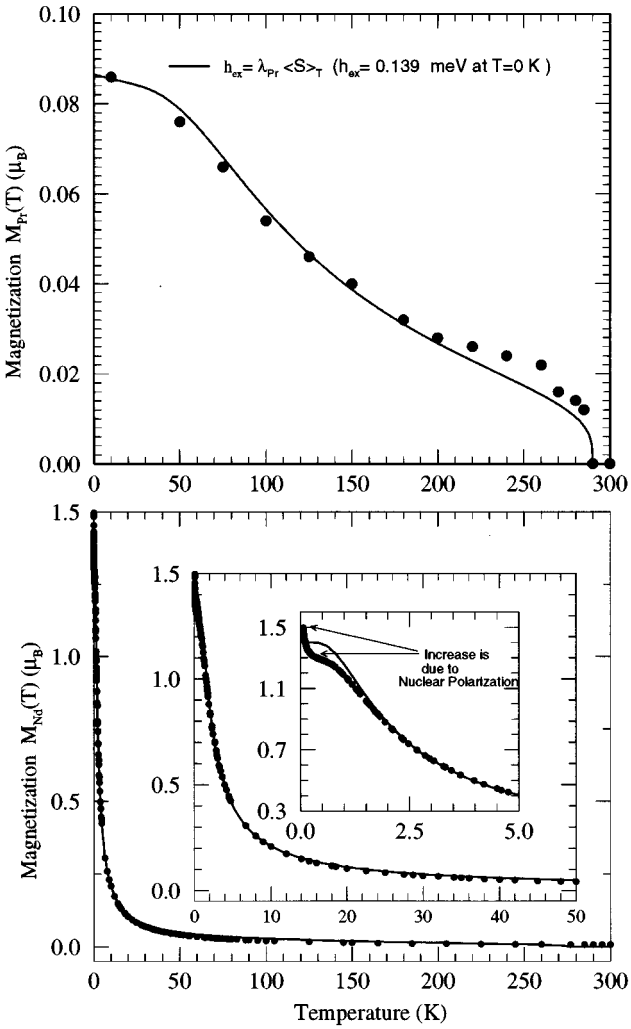

FIG. 7. Fit of experimental magnetization of Nd in NCO (bottom) and Pr in PCO (top) versus temperature (solid circles) compared to theoretical fit (solid line) based on the parameters discussed in the text.

NCO and PCO. We obtained these data from a least-squares fit to a large number of the neutron magnetic Bragg reflections.[58] At about $T=2$ K, the Nd and Pr moments are 1.3 and $0.09\mu_B$, respectively, in good agreement with other studies.[6,33] In order to understand these observed magnetic moments of Nd and Pr we ought to consider the effect of the exchange fields on the R subsystem due to both the Cu ions and the other R ions. However, for the purpose of this section we will consider only the exchange field due to Cu ions. This is a good approximation at all T for PCO and at $T>3$ K for NCO. Accordingly we write the magnitude of the exchange field **h** in Eq. (2), acting on an R ion as

$$h = \lambda_R \langle S \rangle_T, \quad (28)$$

where $\langle S \rangle_T$, the thermally averaged value of the Cu spin is given in Eq. (1). We fix the exchange constants λ_R for R=Nd and Pr by fitting the experimental temperature dependence of the magnetization shown in Fig. 7. The magnetization is calculated from

$$M_R(T) = (1/Z)\mathrm{Tr}(\mu e^{-\mathcal{H}/kT})$$

$$= (1/Z)\sum_m \langle \Psi_m|\mu|\Psi_m\rangle e^{-E_m/kT}, \qquad (29)$$

where E_m and $|\Psi_m\rangle$ are the energies and associated eigenfunctions of $\mathcal{H}$ in Eq. (2), $Z = \Sigma e^{-E_m/kT}$, and μ is the magnetic moment operator divided by μ_B.

The fit to the experimental magnetization is excellent, as shown in Fig. 7. The fitted values of λ_{Nd} and λ_{Pr} are 0.1772 and 0.3474 meV, respectively. These values correspond to $h = 0.071$ and 0.139 meV for Nd and Pr at T=0 K, respectively. For Nd $h = 0.071$ meV gives rise to a splitting of 0.27 meV for the ground-state doublet and $1.27\mu_B$ zero-temperature magnetization, in good agreement with experiments.[4,6,44,45] For NCO, as we shall see in the following sections, the Nd-Nd interactions are also important, particularly at low temperatures, and one has to include them in order to understand the spin waves, etc. Here it is difficult to separate the contribution to Bragg intensities coming from the nuclear polarization, so the data below, say, $T = 3$ K are not as decisive as in some other experiments. For Pr, $h = 0.139$ meV splits the doublets as we discussed perturbatively in Eq. (27). A numerical diagonalization gives values which differ at the percent level from those predicted perturbatively. For $h = 0.139$ meV we find the numerical values of the splitting to be 6.8 μeV for the lower energy doublet and 19.2 μeV for the upper energy doublet. These small splittings may not be observable via inelastic neutron scattering within the current experimental uncertainty, but perhaps they are accessible via other experimental techniques.

Finally, we point out that, as an alternative to Eq. (29), an excellent fit to the data can be obtained by treating only the lowest doublet. In this approximation, the magnetic moment per Nd ion (in units of Bohr magnetons) can be written as

$$M_{\mathrm{Nd}}(T) = M_0 \tanh(\Delta/2kT), \qquad (30)$$

where $\Delta = 2\lambda\langle S\rangle_T x_{11}$. The best fit to the data using this equation yields $\lambda_{\mathrm{Nd}} = 0.17$ meV, $M_0 = 1.34$, and the doublet splitting $\Delta = 0.26$ meV at $T = 0$ K, which are in reasonable agreement with other experimental values.

IV. MAGNETIC REORIENTATION PHASE TRANSITIONS IN NCO

A. Model of interactions

In this section we will construct a model which can explain the sequence of spin reorientation phase transitions observed in NCO and shown in Fig. 2. The model we will introduce is a minimal model, in that one can add to it some other interactions without modifying its main physical characteristics. Some aspects of this model were already proposed in Ref. 26. The model that we treat is described by a Hamiltonian, $\mathcal{H}$,

$$\mathcal{H} = \mathcal{H}_{\mathrm{CEF}} + \mathcal{H}_{\mathrm{Cu}} + \mathcal{H}_{\mathrm{Cu\text{-}Nd}} + \mathcal{H}_{\mathrm{Nd\text{-}Nd}} + V, \qquad (31)$$

where the first four terms describe the Hamiltonian of a single three plane unit (see Fig. 2) and V the coupling between adjacent units. We now discuss the terms in this Hamiltonian in turn. $\mathcal{H}_{\mathrm{CEF}}$ was discussed in Eq. (3).

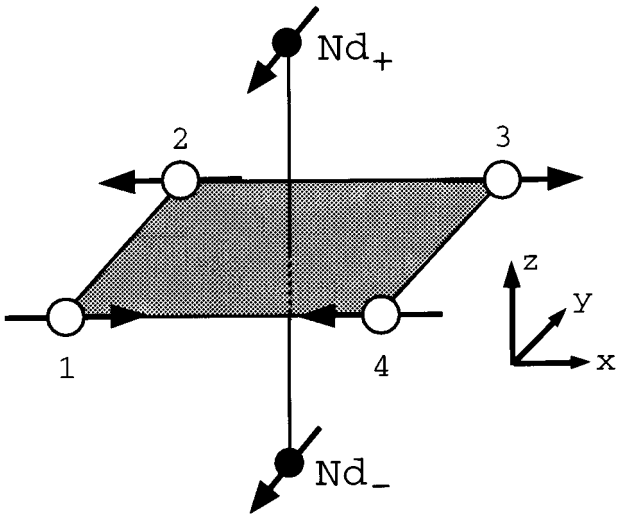

FIG. 8. Nd ions which are nearest neighboring to a plaquette of Cu ions, labeled 1, 2, 3, 4. The Nd ions in planes just above (below) the Cu plane are labeled ''+'' (''−'').

We write

$$\mathcal{H}_{\mathrm{Cu}} = \sum_{\langle ij\rangle \in C} \sum_{\alpha\beta} \mathcal{J}^{ij}_{\alpha\beta} S_{i\alpha} S_{j\beta}, \qquad (32)$$

where α and β label spin components, i and j are Cu site labels, and $\langle ij\rangle \in C$ (and later $\langle ij\rangle \in N$) indicates a summation over pairs of nearest-neighboring Cu (Nd) sites. Now consider the two pairs of Cu sites (1,4) and (1,2) in Fig. 8. The tetragonal symmetry of the lattice implies that

$$\mathcal{J}^{14}_{xx} = \mathcal{J}^{12}_{yy} \equiv \mathcal{J}_\parallel, \quad \mathcal{J}^{14}_{yy} = \mathcal{J}^{12}_{xx} \equiv \mathcal{J}_\perp, \quad \text{and} \quad \mathcal{J}^{14}_{zz} = \mathcal{J}^{12}_{zz} \equiv \mathcal{J}_z, \qquad (33)$$

and all other elements of the tensor $\mathcal{J}$ are zero. Since the spins prefer to lie in the x-y plane, we know that $\mathcal{J}_\parallel + \mathcal{J}_\perp > 2\mathcal{J}_z$. A spin-wave analysis (see Ref. 12 or Sec. V, below) allows us to identify the exchange and anisotropy fields as

$$H_E \equiv \frac{1}{2}(\mathcal{J}_\parallel + \mathcal{J}_\perp) + \mathcal{J}_z,$$

$$H_A \equiv \mathcal{J}_\parallel + \mathcal{J}_\perp - 2\mathcal{J}_z. \qquad (34)$$

We now set $\mathcal{J}_\parallel = \mathcal{J}_\perp$. In Appendix E we show that including the effect of $\mathcal{J}_\parallel \neq \mathcal{J}_\perp$ has only a very small effect on the results for NCO. The values of the exchange constants are fixed by many experiments[1,8] in the cuprates to be $H_E = 130$ meV and $H_A = 0.1$ meV.

We now discuss the remaining interactions between Cu and Nd ions. An important observation concerning the magnetic structure of the three phases of NCO is that all three phases can be considered as being constructed from three-plane (Nd-Cu-Nd) units (labeled A and B in Fig. 2). At each reorientation transition the orientation of unit A with respect to that of unit B changes, but each unit remains intact. Therefore, it seems clear that the interactions which hold each unit together are dominant over the interactions between different

units. This reasoning indicates that the strongest interaction between Cu and Nd ions is that between a plaquette of Cu ions in one plane with the Nd ions directly above (or below) the center of the plaquette, as shown in Fig. 8. However, it is also clear that if this interaction were isotropic, the total effective field on a Nd ion due to a plaquette of Cu ions would sum to zero. Thus we are led to consider an interaction $\mathcal{H}_{\text{Cu-Nd}}$ which consists of anisotropic exchange interactions between the Cu spin 1 and its neighboring Nd ion ''+'' in Fig. 8. We write this interaction as

$$\mathcal{H}_{\text{Cu-Nd}}=\sum_{i\in C}\sum_{j\in N}\sum_{\alpha\beta}K^{ij}_{\alpha\beta}S_{i\alpha}J_{j\beta}, \tag{35}$$

where $i\in C$ ($i\in N$) indicates that the sum over i is over all Cu (Nd) sites, and $J_{j\beta}$ is the β component of the angular momentum operator for the Nd ion on site j. We will keep only the symmetric part of this exchange tensor. (In tetragonal symmetry the effect of the antisymmetric components cancels out when summed over a plaquette of Cu ions.) The existence of a mirror plane (passing through sites 1, 3, and ''+'') implies that the exchange tensor between sites $i=1$ and $j=+$ and (after rotating by 90°) between sites $i=2$ and $j=+$ in Fig. 8 are of the form

$$K^{+,1}=\begin{pmatrix} K_{xx} & K_{xy} & K_{xz} \\ K_{xy} & K_{xx} & K_{xz} \\ K_{xz} & K_{xz} & K_{zz} \end{pmatrix},$$

$$K^{+,2}=\begin{pmatrix} K_{xx} & -K_{xy} & K_{xz} \\ -K_{xy} & K_{xx} & -K_{xz} \\ K_{xz} & -K_{xz} & K_{zz} \end{pmatrix}. \tag{36}$$

We can generate the exchange tensors for other pairs of nearest Nd-Cu neighbors using the symmetry of the lattice. We now use mean-field theory to discuss the effect of this interaction when the spins are constrained to lie in the x-y plane and are specified by giving the vector $\mathbf{S}_1=-\mathbf{S}_2\equiv\mathbf{S}$. The Nd angular momentum of site + is taken to be $\mathbf{J}$ and that of the oppositely oriented Nd moment is $-\mathbf{J}$. Then the mean-field interaction free energy per Nd ion is

$$F_{\text{MF}}=4K_{xy}[S_xJ_y+S_yJ_x]=4K_{xy}SJ\sin(\theta_S+\theta_J), \tag{37}$$

where θ_S (θ_J) is the angle $\mathbf{S}$ ($\mathbf{J}$) makes with the x axis.

Several aspects of this result are noteworthy. First, because of the frustration inherent in an antiferromagnetic plaquette, only the anisotropic interaction of K_{xy} contributes to the total field at an Nd site. Secondly, the resulting interaction has the very unique property that the energy is invariant with respect to rotating one sublattice, say, counterclockwise and the other clockwise. This unusual symmetry leads to a Goldstone mode in the absence of a fourfold anisotropy. Thirdly, we see that when K_{xy} (which by our definition refers to the coupling tensor for the pair Cu,1 and Nd,+) is positive, the orientations of the Nd planes relative to their nearest-neighboring Cu planes are as shown in Fig. 8 (with $\theta_S+\theta_J=-\pi/2$). This ordering is maintained in all three phases of NCO. The angular dependence of this interaction is the same as that of the dipolar interaction,[21] but the interaction required to stabilize the spin structure of NCO is opposite in sign to that for the dipolar interaction. Hence we call this a pseudodipolar interaction. In any event, the magnitude of the pseudodipolar interaction is much larger that that for dipolar interactions between the magnetic moments of the spins.

To summarize: because the orientations of the Nd spins relative to the Cu spins in adjacent planes do not change as one passes through the reorientation transitions, it is reasonable to assume that the interactions discussed above are dominant. Considering only these interactions, one sees that the system naturally condenses into structures in which the three plane units (labeled A and B in Fig. 2) remain intact at all temperatures. For PCO, the sign of K_{xy} must be opposite to that for NCO, because in PCO the relative orientations of the Cu and Pr spins are opposite to what they are in NCO. The actual global spin structure now depends on the smaller couplings between adjacent three plane units.

We now consider the Nd-Nd interactions within a three-plane unit contained in $\mathcal{H}_{\text{Nd-Nd}}$. Since these interactions couple collinear spins, we parametrize them in a slightly simplified way, namely, we set

$$\begin{aligned}\mathcal{H}_{\text{Nd-Nd}}=&\sum_{\langle ij\rangle\in N}[N_\perp(J_{ix}J_{jx}+J_{iy}J_{jy})+N_zJ_{iz}J_{jz}]\\&+\sum_{\langle ij\rangle'}[M_\perp(J_{ix}J_{jx}+J_{iy}J_{jy})+M_zJ_{iz}J_{jz}]\\&+\sum_{\langle ij\rangle''}[O_\perp(J_{ix}J_{jx}+J_{iy}J_{jy})+O_zJ_{iz}J_{jz}],\end{aligned} \tag{38}$$

where $\langle\rangle'$ indicates a sum over nearest-neighboring pairs of Nd spins whose separation vector is parallel to the z axis, and $\langle\rangle''$ a sum over next-nearest-neighbor pairs of Nd spins in the same plane. These couplings are indicated schematically in Fig. 1.

Finally we consider the interaction V between adjacent three-plane units. Referring to Fig. 2 it is natural to imagine that at high temperature (when the Nd moments are very small), the interactions (labeled ''Z'') between Cu ions in different units are dominant, whereas at very low temperature (when the Nd moments are comparable in size to the Cu moments), their interaction (labeled ''X'') dominates because their separation is much less than the Cu-Cu separation. To obtain two spin reorientation transitions we also invoke an intermediate strength interaction (labeled ''Y'') between Cu ions in one unit and Nd ions in an adjacent unit. In the case of the X and Z interactions, it is necessary to invoke an anisotropic pseudodipolar interaction to avoid a cancellation in the mean field. Since the Y interaction involves only pairs of spins, there is no cancellation and we take this interaction to be isotropic. Accordingly, we write the perturbation V which couples adjacent three-plane units in the following form:[59]

$$V = X \sum_{i \in N, j \in N} J_x(i) J_y(j) \Delta_{ij}^{NN} \frac{2x_{ij}y_{ij}}{x_{ij}^2 + y_{ij}^2} + Y \sum_{i \in C, j \in N} \mathbf{S}(i) \cdot \mathbf{J}(j) \Delta_{ij}^{CN} + Z \sum_{i \in C, j \in C} S_x(i) S_y(j) \Delta_{ij}^{CC} \frac{2x_{ij}y_{ij}}{x_{ij}^2 + y_{ij}^2}, \quad (39)$$

where $\mathbf{r}_{ij} \equiv (x_{ij}, y_{ij}, z_{ij})$ is the vector connecting sites i and j, and the Δ factors are either 1 or 0 so as to limit the sums to pairs of sites associated with the coupling constant indicated in Fig. 2: Δ_{ij}^{CC} and Δ_{ij}^{NN} are nonzero only if sites i and j are nearest possible neighbors in nearest neighboring Cu or Nd planes, respectively, and Δ_{ij}^{CN} is nonzero only if sites i and j are nearest possible neighbors in next nearest neighboring Cu and Nd planes. The geometrical factor $x_{ij}y_{ij}/(x_{ij}^2 + y_{ij}^2)$ has the transformation properties characteristic of a pseudodipolar interaction between moments constrained to be perpendicular to the tetragonal c axis.

In Eq. (37) we have already identified the mean-field energy due to the Nd-Cu interaction we believe to be dominant. We now give the mean field free energy per Nd spin associated with those terms in Eq. (31) involving the Nd spin. In writing this result we set $\langle \mathbf{J}(i) \cdot \hat{n}(i) \rangle_T = x_{11} m_N(T)$ for Nd spins and $\langle \mathbf{S}(i) \cdot \hat{n}(i) \rangle_T = \frac{1}{2} m_C(T)$ for Cu spins where $\hat{n}(i)$ is a unit vector along which the ith moment is aligned. [In the absence of quantum zero-point effects, $m_C(T=0) = m_N(T=0) = 1$.] We then find

$$F_{\mathrm{MF}} = -\frac{1}{2}[4K_{xy} - \sigma Y] x_{11} m_N(T) m_C(T) - \frac{1}{2}(4N_\perp - M_\perp - 4O_\perp + 4\sigma X) x_{11}^2 m_N(T)^2, \quad (40)$$

where $\sigma = 1$ for phases I and III and $\sigma = -1$ for phase II. Within this approximation the splitting of the lowest Nd doublet is

$$\Delta(T) = -2\partial F_{\mathrm{MF}}/\partial m_N(T) = [4K_{xy} - \sigma Y] x_{11} m_C(T) + (8N_\perp - 2M_\perp - 8O_\perp + 8\sigma X) x_{11}^2 m_N(T) \equiv \Delta_C + \Delta_N, \quad (41)$$

where $\Delta_C = (4K_{xy} - \sigma Y) x_{11}$ is the part of the splitting of the lowest Nd doublet due to the exchange field of the Cu ions and Δ_N is the remaining part of the splitting due to the Nd-Nd interactions. Comparing to Eq. (2), we see that

$$h = 2\Delta / x_{11}. \quad (42)$$

The term in Eq. (41) proportional to K_{xy} is the dominant one. The next largest terms are those in M, N, and O, which are intraunit interactions. The effect of the weaker interactions between three-plane units on the mean-field energy will be neglected.

B. Mechanism for reorientation transitions

We now consider the perturbative contribution, δF_{uc}, to the mean-field free energy per magnetic unit cell from the coupling V between adjacent three-plane units. In analogy to Eq. (40) we have that

$$\delta F_{uc} = -4\sigma Z m_C(T)^2 [1 + y\psi(T) + 4x\psi(T)^2] \equiv -4\sigma Z m_C(T)^2 \Phi(T), \quad (43)$$

where $y = -Y/Z$, $x = X/Z$, $\psi(T) = x_{11} m_N(T)/m_C(T)$, and σ is $+1$ in phases I and III and is -1 in phase II. It is clear that the free energy is minimized by the structure of phases I and III if $Z\Phi(T)$ is positive and by that of phase II if $Z\Phi(T)$ is negative. In order to obtain phase II between the two reorientation transition temperatures, $T_< = 30$ K and $T_> = 75$ K, it is necessary that $Z > 0$ and

$$x = \frac{1}{4\psi(T_<)\psi(T_>)} = 51, \quad y = -\frac{\psi(T_>) + \psi(T_<)}{\psi(T_<)\psi(T_>)} = -31, \quad (44)$$

where we used Eqs. (1) and (30) to construct $m_C(T)$ and $m_N(T)$ which we used to obtain the above numerical values. (These equations give values which are essentially equivalent to experimental ones.) We reiterate that the magnetic dipole-dipole interaction does not explain the stability of these phases.[60] Since $m_N(T)$ is small at both transitions (see Fig. 7), it is clear that $x \gg -y \gg 1$ or $X \gg Y \gg Z$. As we have mentioned, the plausibility of this condition is obvious from the geometry, shown in Fig. 2.

We can also now include the effect of these small perturbations on the Nd doublet splitting. Referring to Eqs. (40) and (42) we see that the mean field at the Nd site will have a jump at each of the two reorientation transitions (where σ changes sign), and indeed the Raman data[44] shows such a discontinuity. However, the magnitude of the discontinuity is not easy to obtain from the data, because the data gives directly only the sum of the splittings of the doublets of the initial and final Raman states. In principle, a determination of the jumps in the doublet splitting at these transitions would fix the magnitudes of X, Y, and Z, since their ratios are already fixed by Eq. (44). In any event the sign of the discontinuity is not consistent with only magnetic dipole-dipole interactions. It remains to consider what this explanation implies for PCO, if we assume that the values of x and y for PCO are the same as those for NCO. Note from Figs. 2 and 3 that PCO and NCO (in phase I) differ in the three-plane units because the Cu spins are reversed in PCO from their directions in NCO. That means that to treat PCO we should change the signs of the $m_C(T)$'s. This change is equivalent to changing the sign of Y, or equivalently, the sign of y. However, then both x and y are positive and Φ is positive at all temperatures and the phase analogous to NCO phase I [i.e., the actual structure of PCO shown in Fig. 3(a)] is the stable one. This argument is clearly rather speculative, because then one would have to assert that under high pressure (when PCO does have a sequence of spin reorientations[46]) the constant y changes sign.

V. SPIN WAVES IN NCO

A. General discussion

In this section we use our model to calculate the spin-wave spectrum of NCO. Although Thalmeier[22] has given a very thorough treatment of the spin-wave spectrum of NCO, there are some aspects of his model that we find unsatisfactory, as we discuss below. In addition, his basic assumption that the dynamics of the Cu spins can be ignored is only appropriate as long as the wave vector is not too small. Thus his approach, although useful in many respects, is not appropriate for a discussion of the zero wave-vector modes. For that purpose we have had recourse to a simplified 2D model which enables us to easily take account of the motion of the Cu spins, the details of their anisotropic coupling to the Nd sublattices, and the anisotropy of the Nd spins caused by the crystalline electric field. In the future, it may be of interest to extend our calculation to a full 3D model.

The Cu-Cu interactions are taken to be as in other cuprates. The most important Cu-Nd interaction is fixed by the high-temperature limit of the Nd doublet splitting. We have fixed the Nd-Nd interactions to get reasonable agreement with the experimental results of Henggeler *et al.*[18] for the spin-wave energies throughout the Brillouin zone. Particularly simple results are obtained at zero wave vector. The temperature-dependent energies of the optical modes agree well with the experimental values of Ivanov *et al.*[17] We also predict the energy gap in the acoustic mode due to the small fourfold in-plane anisotropy.

The present discussion will assume the structure of phase I, although as will be seen, most of our results apply to the spectrum in all three phases. As discussed in Sec. IV, we may consider the entire system to be built up of weakly interacting sets of planes, each set consisting of a Cu plane with one Nd plane above it and another below it. Thus, for most purposes it suffices to consider a 2D model consisting of a single set of Nd-Cu-Nd planes. In this 2D model the spin-wave spectrum has six branches, and the energies of the modes are functions of the 2D wave vector $\mathbf{q_2}$. In the actual 3D model, the spin-wave spectrum has 12 branches and each mode energy is a function of the 3D wave vector, $\mathbf{q}\equiv(\mathbf{q}_2,q_z)$. The actual spin-wave spectrum[18] consisting of 12 branches has essentially no dispersion with respect to q_z because the coupling between one Nd-Cu-Nd set of planes and the next such set of planes is relatively weak. Since the 3D unit cell contains two nearly noninteracting sets of planes, the 12 branch spectrum at some value of $\mathbf{q}\equiv(\mathbf{q}_2,q_z)$ is the union of one six branch spectrum evaluated at $\mathbf{q}_2$ and another six branch spectrum evaluated at $R\mathbf{q}_2$, where R is a rotation by 90° about the z axis. Therefore almost all information is contained in our simplified 2D model of one set of Nd-Cu-Nd planes. The unit cell for this model is shown in Fig. 9.

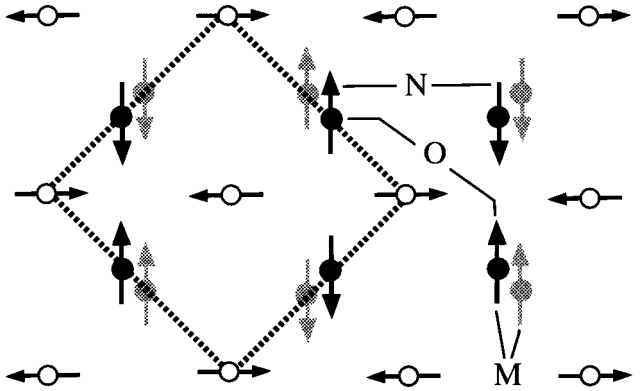

FIG. 9. 2D unit cell (indicated by the dashed square) for our simplified model of spin waves in NCO. The open circles are Cu ions and the filled ones Nd ions. The darker (lighter) Nd arrows represent the Nd spins in planes just above (below) the Cu planes. The Nd-Nd interactions scaled by the tensors **M**, **N**, and **O** are indicated.

The exchange interactions for the model that we treat are those described previously in Sec. IV, so that the Hamiltonian is

$$\mathcal{H}=\mathcal{H}_{\mathrm{CEF}}+\sum_{\langle ij\rangle\in C}[\mathcal{J}_{\perp}(S_{ix}S_{jx}+S_{iy}S_{jy})+\mathcal{J}_z S_{iz}S_{jz}]+\sum_{i\in \mathrm{C}}\sum_{j\in N}\sum_{\alpha\beta}K_{\alpha\beta}S_{i\alpha}J_{j\beta}+\sum_{\langle ij\rangle\in N}[N_{\perp}(J_{ix}J_{jx}+J_{iy}J_{jy})+N_z J_{iz}J_{jz}]$$
$$+\sum_{\langle ij\rangle'}[M_{\perp}(J_{ix}J_{jx}+J_{iy}J_{jy})+M_z J_{iz}J_{jz}]+\sum_{\langle ij\rangle''}[O_{\perp}(J_{ix}J_{jx}+J_{iy}J_{jy})+O_z J_{iz}J_{jz}]. \quad (45)$$

The first line contains the first three terms in Eq. (31) and the remaining lines contain the Nd-Nd interactions shown in Figs. 1 and 9. To discuss spin waves we will use the Holstein-Primakoff (HP) transformation for the Cu spins and a similar transformation to reproduce the dynamics of the Nd spin within the lowest crystal-field doublet. This procedure will lead us to a bosonic Hamiltonian in which terms higher than quadratic in bosonic variables are neglected and in which quadratic excitations involving higher crystal-field states are also ignored.

B. Transformation to bosons

The transformation to bosons is obtained by the following general algorithm for a bilinear interaction involving an operator **R** on one site and **S** on another site. Write

$$\mathbf{RS}=\langle\mathbf{R}\rangle\langle\mathbf{S}\rangle+\langle\mathbf{S}\rangle\delta\mathbf{R}+\delta\mathbf{S}\langle\mathbf{R}\rangle+\delta\mathbf{R}\delta\mathbf{S}, \quad (46)$$

where $\langle\rangle$ indicates an average in the mean-field ground state, and $\delta\mathbf{R}=\mathbf{R}-\langle\mathbf{R}\rangle$. By expressing $\delta\mathbf{R}$ and $\delta\mathbf{S}$ in terms of bosonic excitations about the mean-field ground state one

can obtain an expression for the bilinear interaction in terms of bosonic variables. (In the case of isotropic spins, this prescription is identical to that leading to the HP transformation.)

There are two sublattices within a copper plane which we call a and b. In the ground state the a sublattice spins $\langle \mathbf{S}^a \rangle$ point in the $+x$ direction, while the b spins $\langle \mathbf{S}^b \rangle$ point in the $-x$ direction. The HP transformation may be written as

$$S_x^a = S - a^\dagger a, \quad S_x^b = -S + b^\dagger b, \tag{47a}$$

$$S_y^a = \sqrt{S/2}(a^\dagger + a), \quad S_y^b = \sqrt{S/2}(b^\dagger + b), \tag{47b}$$

$$S_z^a = \sqrt{S/2}(a^\dagger - a), \quad S_z^b = -i\sqrt{S/2}(b^\dagger - b). \tag{47c}$$

There are two identically ordered Nd planes, one above, the other below the Cu plane. We denote the sublattices above (below) the Cu plane with moments along the $-y$ direction as n_+ (n_-) and the other Nd sublattice above (below) the Cu plane as m_+ (m_-). For the moment we consider a spin in one of the n sublattices. In the presence of the exchange field due to the other ions its lowest doublet will be split into a ground state $|g\rangle$ and an excited state $|e\rangle$. Following the prescription given above we write

$$J_\alpha = \langle g|J_\alpha|g\rangle + \sum_f \left(\langle f|J_\alpha|g\rangle n_f^\dagger + \langle g|J_\alpha|f\rangle n_f + (\langle f|J_\alpha|f\rangle - \langle g|J_\alpha|g\rangle) n_f^\dagger n_f\right) + \sum_{f \neq f'} \langle f|J_\alpha|f'\rangle n_f^\dagger n_{f'}, \tag{48}$$

where we define $n_f^\dagger|g\rangle = |f\rangle$, and $|f\rangle$ and $|f'\rangle$ are excited states. We henceforth keep only bosonic excitations within the lowest doublet. Thus in Eq. (48) the last term is dropped and in the first term the only excited state that enters is $|e\rangle$ and we let n denote n_e. Note that in principle the admixture of higher crystal-field states into $|g\rangle$ and $|e\rangle$ is taken into account exactly. However, we did not calculate the moments of the Nd ions self-consistently, as this prescription requires. The effect of self-consistency is entirely negligible here.

For the n sublattice (with Nd spins in the $-y$ direction) we have,

$$\begin{pmatrix} \langle e| \\ \langle g| \end{pmatrix} \mathbf{J}(|e\rangle|g\rangle) = \left[j_x \sigma_x, \frac{1}{2}(j_{y+} + j_{y-})I + \frac{1}{2}(j_{y+} - j_{y-})\sigma_z, -j_z \sigma_y \right], \tag{49}$$

where σ_α is a Pauli matrix and I is the unit 2×2 matrix. In Appendix D we develop expressions for the states $|g\rangle$ and $|e\rangle$ of the lowest doublet in the presence of an exchange field h, as power series in h. We have carried these expansions up to order h^3 to obtain results for the constants in Eqs. (D7)–(D11). The anisotropic response of the Nd ion to a magnetic field is due to the differences in the values of j_x, j_{y+}, $-j_{y-}$, and j_z. Setting all of them equal to each other ($j_x = j_z = j_{y+} = -j_{y-}$) will make this an isotropic spin-1/2 system. The expansions of the j's have to be carried to at least second order in h to get anisotropy within the x-y plane. At that order $j_{y+} = -j_{y-} \equiv j_y = x_{11} + O(h^2)$ and Appendix D gives $(j_x + j_y)/2 \approx 1.886$. The anisotropy in the plane is governed by the value of $j_y - j_x$, which is of order h^2 and which is evaluated in Appendix D to be 1.38×10^{-4}. Thus Eq. (48) becomes

$$J_y = \langle g|J_y|g\rangle + (\langle e|J_y|e\rangle - \langle g|J_y|g\rangle) n^\dagger n = -j_y + 2j_y n^\dagger n, \tag{50a}$$

$$J_x = \langle e|J_x|g\rangle n^\dagger + \langle g|J_x|e\rangle n = j_x(n^\dagger + n), \tag{50b}$$

$$J_z = \langle e|J_z|g\rangle n^\dagger + \langle g|J_z|e\rangle n = i j_z(n^\dagger - n). \tag{50c}$$

In the m sublattices change the sign of y and z components and replace n with m.

The splitting of the doublet Δ (when all ions are initially in their ground state) is

$$\begin{aligned} \Delta &= \sum_j 2j_y K_{xy} \langle S_a^j \rangle + 2j_y^2 \sum_j N_\perp - 2j_y^2 \sum_j M_\perp - 2j_y^2 \sum_j O_\perp \\ &= 4K_{xy} j_y + (8N_\perp - 2M_\perp - 8O_\perp) j_y^2 \\ &\equiv \Delta_C + \Delta_N . \end{aligned} \tag{51}$$

Here the sums over j encompass the shell of neighbors associated with the exchange interaction in question. This result differs from Eq. (41) because the interactions between different three-plane units are not included in the present model. Also here we replace x_{11} by j_y. This replacement has only a small effect numerically, but to treat the R anisotropy correctly we have to include the dependence of the wave functions on h.

C. Spin waves

After the above-described transformation to bosons is used, the exchange Hamiltonian becomes

$$\mathcal{H}=\left(H_E+\frac{1}{2}H_A+2\Delta\right)\left(\sum_{\mathbf{p}} a_{\mathbf{p}}^{\dagger}a_{\mathbf{p}}+\sum_{\mathbf{r}} b_{\mathbf{r}}^{\dagger}b_{\mathbf{r}}\right)+\frac{1}{8}H_A\sum_{\mathbf{p},\mathbf{r}} \gamma_{\mathbf{pr}}(a_{\mathbf{p}}^{\dagger}b_{\mathbf{r}}+b_{\mathbf{r}}^{\dagger}a_{\mathbf{p}})+\frac{1}{4}H_E\sum_{\mathbf{p},\mathbf{r}} \gamma_{\mathbf{pr}}(a_{\mathbf{p}}^{\dagger}b_{\mathbf{r}}^{\dagger}+a_{\mathbf{p}}b_{\mathbf{r}})$$

$$+\sum_{\alpha}\sum_{\mathbf{s}_\alpha\mathbf{t}_\alpha}\{\delta_{\mathbf{t}_\alpha,\mathbf{s}_\alpha}\Delta(n_{\mathbf{s}_\alpha}^{\dagger}n_{\mathbf{s}_\alpha}+m_{\mathbf{t}_\alpha}^{\dagger}m_{\mathbf{t}_\alpha})+\gamma_{\mathbf{t}_\alpha,\mathbf{s}_\alpha}[(N_\perp j_x^2+N_z j_z^2)(n_{\mathbf{s}_\alpha}^{\dagger}n_{\mathbf{t}_\alpha}^{\dagger}+n_{\mathbf{t}_\alpha}n_{\mathbf{s}_\alpha})+(N_\perp j_x^2-N_z j_z^2)(n_{\mathbf{s}_\alpha}^{\dagger}n_{\mathbf{t}_\alpha}+n_{\mathbf{t}_\alpha}^{\dagger}n_{\mathbf{s}_\alpha})]$$

$$+\gamma_{\mathbf{t}_\alpha,\mathbf{s}_\alpha}^{(2)}[(O_\perp j_x^2-O_z j_z^2)(n_{\mathbf{s}_\alpha}^{\dagger}n_{\mathbf{t}_\alpha}^{\dagger}+n_{\mathbf{t}_\alpha}n_{\mathbf{s}_\alpha})+(O_\perp j_x^2+O_z j_z^2)(n_{\mathbf{s}_\alpha}^{\dagger}n_{\mathbf{t}_\alpha}+n_{\mathbf{t}_\alpha}^{\dagger}n_{\mathbf{s}_\alpha})]\}+\sum_{\mathbf{u}}[(M_\perp j_x^2-M_z j_z^2)(n_{\mathbf{u}_+}^{\dagger}n_{\mathbf{u}_-}^{\dagger}+n_{\mathbf{u}_+}n_{\mathbf{u}_-})$$

$$+(M_\perp j_x^2+M_z j_z^2)(n_{\mathbf{u}_+}^{\dagger}n_{\mathbf{u}_-}+n_{\mathbf{u}_+}^{\dagger}n_{\mathbf{u}_-})]+\sum_{\alpha}\sum_{\mathbf{p},\mathbf{s}_\alpha}(K_{\mathbf{p},\mathbf{s}_\alpha}^{(0)}a_{\mathbf{p}}^{\dagger}n_{\mathbf{s}_\alpha}+K_{\mathbf{p},\mathbf{s}_\alpha}^{(1)}a_{\mathbf{p}}^{\dagger}n_{\mathbf{s}_\alpha}^{\dagger}+\text{H. c.})+\sum_{\alpha}\sum_{\mathbf{p},\mathbf{t}_\alpha}(K_{\mathbf{p},\mathbf{t}_\alpha}^{(0)}a_{\mathbf{p}}^{\dagger}m_{\mathbf{t}_\alpha}+K_{\mathbf{p},\mathbf{t}_\alpha}^{(1)}a_{\mathbf{p}}^{\dagger}m_{\mathbf{t}_\alpha}^{\dagger}$$

$$+\text{H. c.})+\sum_{\alpha}\sum_{\mathbf{r},\mathbf{s}_\alpha}(K_{\mathbf{r},\mathbf{s}_\alpha}^{(0)}b_{\mathbf{r}}^{\dagger}n_{\mathbf{s}_\alpha}+K_{\mathbf{r},\mathbf{s}_\alpha}^{(1)}b_{\mathbf{p}}^{\dagger}n_{\mathbf{s}_\alpha}^{\dagger}+\text{H. c.})+\sum_{\alpha}\sum_{\mathbf{r},\mathbf{t}_\alpha}(K_{\mathbf{r},\mathbf{t}_\alpha}^{(0)}b_{\mathbf{r}}^{\dagger}m_{\mathbf{t}_\alpha}+K_{\mathbf{r},\mathbf{t}_\alpha}^{(1)}b_{\mathbf{r}}^{\dagger}m_{\mathbf{t}_\alpha}^{\dagger}+\text{H. c.}), \tag{52}$$

where the exchange field, H_E, and anisotropy field, H_A, were defined in Eqs. (34). Also $\mathbf{p}$ refers to sites on the a sublattice, $\mathbf{r}$ the b sublattice, $\mathbf{s}_\alpha$ the n_α sublattice, and $\mathbf{t}_\alpha$ the m_α sublattice, where the subscript α assumes the values $+$ and $-$ for the Nd sublattices, respectively, above and below the Cu plane. In the third line of the above equation, the sum over $\mathbf{u}$ is taken so that $\mathbf{u}_+$ ranges over all sites in the n_+ and m_+ sublattices. Also $\delta_{\mathbf{u},\mathbf{v}}$ is unity if $\mathbf{u}=\mathbf{v}$, $\gamma_{\mathbf{u},\mathbf{v}}$ is unity if $\mathbf{u}$ and $\mathbf{v}$ are nearest neighbors in the same plane and is zero otherwise, and $\gamma_{\mathbf{u},\mathbf{v}}^{(2)}$ is unity if $\mathbf{u}$ and $\mathbf{v}$ are next-nearest neighbors in the same plane and is zero otherwise. We now specify the interaction constants $K_{\mathbf{u},\mathbf{v}}^{(0)}$, where $\mathbf{u}$ is a Cu site and $\mathbf{v}$ a nearest-neighboring Nd site. For this purpose it is convenient to introduce the notation that $\mathbf{v}=\mathbf{u}+a\vec{\delta}$, where the x and y components of $\vec{\delta}$ are each of magnitude 1/2 and the z component is $\pm\beta$. Then we write $K_{\mathbf{u},\mathbf{v}}^{(n)}\equiv K_{\mathbf{u}}^{(n)}(\vec{\delta})$. We have

$$K_{\mathbf{p}}^{(n)}\left(\frac{1}{2},\frac{1}{2},\beta\right)=K_{\mathbf{p}}^{(n)}\left(-\frac{1}{2},-\frac{1}{2},\beta\right)^*$$

$$=-K_{\mathbf{p}}^{(n)}\left(-\frac{1}{2},\frac{1}{2},\beta\right)=-K_{\mathbf{p}}^{(n)}\left(\frac{1}{2},-\frac{1}{2},\beta\right)^*$$

$$\equiv K_n, \tag{53}$$

where

$$K_0=\frac{1}{2}(K_{xy}j_x+K_{zz}j_z)+\frac{1}{2}iK_{xz}(j_x-j_z), \tag{54a}$$

$$K_1=\frac{1}{2}(K_{xy}j_x-K_{zz}j_z)+\frac{1}{2}iK_{xz}(j_x+j_z). \tag{54b}$$

The other coupling constants can be obtained using the relations $K_{\mathbf{u}}^{(n)}(\vec{\delta})=K_{\mathbf{u}}^{(n)}(-\vec{\delta})$ and $K_{\mathbf{r}}^{(n)}(\vec{\delta})=K_{\mathbf{p}}^{(n)}(\vec{\delta})^*$.

To obtain the spin-wave spectrum we introduce spatial Fourier transforms via

$$c_i^{\dagger}(\mathbf{q})=N_{\text{uc}}^{-1/2}\sum_{\mathbf{r}\in i} c_{\mathbf{r}}^{\dagger}e^{-i\mathbf{q}\cdot\mathbf{r}}, \tag{55}$$

where N_{uc} is the number of unit cells in the system, $\mathbf{r}\in i$ indicates that $\mathbf{r}$ is summed over all sites in the ith sublattice, and the sublattices are labeled so that 1,2,3,4,5,6 correspond, respectively, to a,b,n_+,m_+,n_-,m_-. Thus, if $\mathbf{r}$ is in the a sublattice, then $c_{\mathbf{r}}^{\dagger}=a_{\mathbf{r}}^{\dagger}$. With this notation we have

$$\mathcal{H}=\sum_{\mathbf{q}}\left\{\sum_{ij}A_{ij}(\mathbf{q})c_i^{\dagger}(\mathbf{q})c_j(\mathbf{q})\right.$$

$$\left.+\frac{1}{2}\sum_{ij}[B_{ij}(\mathbf{q})c_i^{\dagger}(\mathbf{q})c_j^{\dagger}(\mathbf{q})+\text{H. c.}]\right\}, \tag{56}$$

where

$$\mathbf{A}=\begin{bmatrix} H_E+\frac{1}{2}H_A+2\Delta_C & \frac{1}{4}H_A(c_x+c_y) & (2K_0e_xe_y)' & -(2K_0e_y/e_x)' & (2K_0^*e_xe_y)' & -(2K_0^*e_y/e_x)' \\ \frac{1}{4}H_A(c_x+c_y) & H_E+\frac{1}{2}H_A+2\Delta_C & -(2K_0^*e_y/e_x)' & (2K_0^*e_xe_y)' & -(2K_0e_y/e_x)' & (2K_0e_xe_y)' \\ (2K_0e_xe_y)' & -(2K_0^*e_y/e_x)' & \Delta+4O^+c_xc_y & 2(c_x+c_y)N^- & M^+ & 0 \\ -(2K_0e_y/e_x)' & (2K_0^*e_xe_y)' & 2(c_x+c_y)N^- & \Delta+4O^+c_xc_y & 0 & M^+ \\ 2(K_0^*e_xe_y)' & -(2K_0e_y/e_x)' & M^+ & 0 & \Delta+4O^+c_xc_y & 2(c_x+c_y)N^- \\ -(2K_0^*e_y/e_x)' & (2K_0e_xe_y)' & 0 & M^+ & 2(c_x+c_y)N^- & \Delta+4O^+c_xc_y \end{bmatrix} \tag{57}$$

$$\mathbf{B}=\begin{bmatrix} 0 & \frac{1}{2}H_E(c_x+c_y) & (2K_1e_xe_y)' & -(2K_1e_y/e_x)' & (2K_1^*e_xe_y)' & -(2K_1^*e_y/e_x)' \\ \frac{1}{2}H_E(c_x+c_y) & 0 & -(2K_1^*e_y/e_x)' & (2K_1^*e_xe_y)' & -(2K_1e_y/e_x)' & (2K_1e_xe_y)' \\ (2K_1e_xe_y)' & -(2K_1^*e_y/e_x)' & 4O^-c_xc_y & 2(c_x+c_y)N^+ & M^- & 0 \\ -(2K_1e_y/e_x)' & (2K_1^*e_xe_y)' & 2(c_x+c_y)N^+ & 4O^-c_xc_y & 0 & M^- \\ 2(K_1^*e_xe_y)' & -(2K_1e_y/e_x)' & M^- & 0 & 4O^-c_xc_y & 2(c_x+c_y)N^+ \\ -(2K_1^*e_y/e_x)' & (2K_1e_xe_y)' & 0 & M^- & 2(c_x+c_y)N^+ & 4O^-c_xc_y \end{bmatrix}, \tag{58}$$

where $c_x=\cos aq_x$, $c_y=\cos aq_y$, $e_x=\exp(iaq_x/2)$, $e_y=\exp(iaq_y/2)$, $(X)'\equiv \mathrm{Re}X$, and $X^{\pm}=(X_\perp j_x^2 \pm X_z j_z^2)$, where X stands for M, N, or O. The eigenvalues of the matrix $(\mathbf{A}+\mathbf{B})(\mathbf{A}-\mathbf{B})$ give the squares of the energy of the normal modes:

$$(\mathbf{A}+\mathbf{B})(\mathbf{A}-\mathbf{B})\chi_\tau(\mathbf{q})=\omega(\mathbf{q})^2\chi_\tau(\mathbf{q}). \tag{59}$$

The eigenvalues are invariant with respect to the operation $\mathbf{q}\rightarrow-\mathbf{q}$, as expected in view of time-reversal symmetry. To see this explicitly note that changing the sign of $\mathbf{q}$ is equivalent to interchanging rows and columns 3 and 5 and rows and columns 4 and 6.

The complete model for the whole lattice will have two layers of our 2D model per unit cell, with one rotated by 90° about the z axis (so that the a sublattice spins now point in the $-y$ direction, and the b sublattice in the $+y$ direction, etc.). From Eqs. (57) and (58) one can see that when K_0 is real (i.e., when $K_{xz}=0$), the spectrum is invariant under this $\mathbf{R}_4$ operation. Even when K_{xz} is nonzero, this invariance holds for wave vectors in high-symmetry directions. Thus in the complete model the spectrum consists of six nearly doubly degenerate modes which are split by weak couplings between adjacent three-plane units.

D. Normal modes at q=0 and on the zone boundary

For $q=0$, we have the simpler forms

$$\mathbf{A}=\begin{bmatrix} H_E+\frac{1}{2}H_A+2\Delta_C & \frac{1}{2}H_A & 2K_0' & -2K_0' & 2K_0' & -2K_0' \\ \frac{1}{2}H_A & H_E+\frac{1}{2}H_A+2\Delta_C & -2K_0' & 2K_0' & -2K_0' & 2K_0' \\ 2K_0' & -2K_0' & \Delta+4O^+ & 4N^- & M^+ & 0 \\ -2K_0' & 2K_0' & 4N^- & \Delta+4O^+ & 0 & M^+ \\ 2K_0' & -2K_0' & M^+ & 0 & \Delta+4O^+ & 4N^- \\ -2K_0' & 2K_0' & 0 & M^+ & 4N^- & \Delta+4O^+ \end{bmatrix}, \tag{60}$$

$$\mathbf{B}=\begin{bmatrix} 0 & H_E & 2K_1' & -2K_1' & 2K_1' & -2K_1' \\ H_E & 0 & -2K_1' & 2K_1' & -2K_1' & 2K_1' \\ 2K_1' & -2K_1' & 4O^- & 4N^+ & M^- & 0 \\ -2K_1' & 2K_1' & 4N^+ & 4O^- & 0 & M^- \\ 2K_1' & -2K_1' & M^- & 0 & 4O^- & 4N^+ \\ -2K_1' & 2K_1' & 0 & M^- & 4N^+ & 4O^- \end{bmatrix}. \tag{61}$$

We can immediately identify several eigenmodes. For instance $|1\rangle$ and $|2\rangle$ are given, respectively, by the upper and lower choices of sign in $(n_+ + m_+ \pm n_- \pm m_-)/2$. The energy of these modes is

$$\omega_\pm^2 = (\Delta + 4N^- + 4O^+ \pm M^+)^2 - (4N^+ + 4O^- \pm M^-)^2$$
$$\approx \Delta^2 + 2\Delta j_x^2[4O_\perp + 4N_\perp \pm M_\perp]. \tag{62}$$

The other simple rare-earth mode is $|3\rangle = (n_+ - m_+ - n_- + m_-)/2$, with

$$\omega_3^2 = (\Delta + 4O^+ - 4N^- - M^+)^2 - (4O^- - 4N^+ - M^-)^2$$
$$\approx \Delta^2 + 2\Delta j_x^2[4O_\perp - 4N_\perp - M_\perp]. \tag{63}$$

These three modes have energy which is split from Δ by the Nd-Nd interactions.

The other three modes involve the Cu spins. One of these is the out-of-plane Cu mode: $|4\rangle = (a+b)/\sqrt{2}$. For it

$$\omega_4^2 = (H_E + H_A + 2\Delta_C)^2 - H_E^2 \approx 2H_E(H_A + 2\Delta_C). \tag{64}$$

The remaining two modes are linear combinations of excitations on the Cu, $|5\rangle = (a-b)/\sqrt{2}$ and on the Nd, $|6\rangle = (n_+ - m_+ + n_- - m_-)/2$. In this subspace we have

$$A = \begin{bmatrix} H_E + 2\Delta_C & 2\sqrt{2}(K_{xy} j_x + K_{zz} j_z) \\ 2\sqrt{2}(K_{xy} j_x + K_{zz} j_z) & \Delta + F_\perp + F_z \end{bmatrix},$$
$$B = \begin{bmatrix} -H_E & 2\sqrt{2}(K_{xy} j_x - K_{zz} j_z) \\ 2\sqrt{2}(K_{xy} j_x - K_{zz} j_z) & F_\perp - F_z \end{bmatrix}, \tag{65}$$

where $F_\perp = (M_\perp - 4N_\perp + 4O_\perp) j_x^2$ and $F_z = (M_z - 4N_z + 4O_z) j_z^2$ and we used Eqs. (54). We denote the two eigenvalues of the matrix $(\mathbf{A}+\mathbf{B})(\mathbf{A}-\mathbf{B})$ as $\omega_>^2$ and $\omega_<^2$ and find

$$\omega_>^2 \approx 4H_E \Delta_C. \tag{66}$$

Neglecting terms of order j_z^2 and using the values of the parameters given in Sec. V G, below, we have

$$\omega_< = \Delta\left(1 - \frac{j_x^2}{j_y^2}\right)^{1/2} \approx 3.7\ \mu\text{eV}. \tag{67}$$

We can understand these results in the following manner. Since the Nd's mix with the Cu's only via the uniform Nd excitation ($|6\rangle$), we have three Nd modes whose energy (ω_k for $k=1,2,3$) is approximately Δ. The energy differences between these modes is caused by (and therefore is a measure of) the Nd-Nd interactions. One of the other modes is an out-of-plane Cu mode which would have energy $\approx \sqrt{2H_A H_E}$ in the absence of the Nd ions. The Nd ions contribute a staggered field of energy $2\Delta_C$, so that H_A is here replaced by $H_A + 2\Delta_C$. Another mode is an in-plane optical mode in which the staggered field is $2\Delta_C$ but this mode does not involve the out-of-plane anisotropy, H_A. This mode has energy $\omega_>$ given in Eq. (66). Finally, there is an acoustic mode which involves the fourfold anisotropy. We may define a phenomenological fourfold anisotropy constant, k_4 via

$$E = -\frac{1}{8} k_4 \cos 4\phi, \tag{68}$$

where E is the ground-state energy and ϕ is the angle in the x-y plane which the exchange field makes with a [100] direction. We will identify k_4 by finding the ground-state energy for small ϕ when the exchange Hamiltonian is

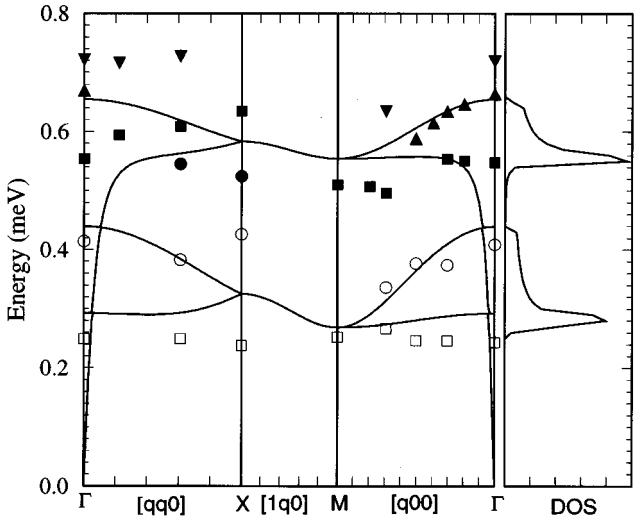

FIG. 10. Full curves are the energies (at $T=0$) of the low-energy modes with respect to the 2D wave vector calculated using the values of the parameters as given in Eqs. (84)–(88). In the full 3D model, each of these modes gives rise to two modes whose splitting is determined mostly by the small coupling between adjacent sets of three planes. This coupling is neglected in the 2D model. The squares, circles, and triangles are mode energies determined by the inelastic neutron experiments of Ref. 18. (The data of Ref. 19 is similar to that shown here.) Note that the calculations predict a strong dispersion of the acoustic mode at small wave vector. At the far right we show the density of states (DOS) obtained from an evaluation over the entire 2D Brillouin zone.

$V_{ex} \equiv -4K_{xy}\hat{n}\cdot\mathbf{J}$ with $\hat{n}=(\sin\phi,\cos\phi,0)$. Thus $k_4=\partial E/\partial\phi^2|_{\phi=0}$. Using the matrix elements of the doublet given in Eq. (50a), we write the exchange Hamiltonian in terms of Pauli matrices within the lowest doublet as

$$V_{ex}=4K_{xy}[-j_y\cos\phi\sigma_z-\sin\phi j_x\sigma_x]. \tag{69}$$

For small ϕ the ground-state energy is

$$E_0=4K_{xy}\left[-j_y\left(1-\frac{1}{2}\phi^2\right)-j_x^2\phi^2/(2j_y)\right]. \tag{70}$$

This result suggests that we make the identification

$$k_4=(\Delta/2)(1-j_x^2/j_y^2)\approx\Delta(1-j_x/j_y)=7.3\times10^{-5}\Delta \tag{71}$$

and we write

$$\omega_<^2=2k_4\Delta\approx1.5\times10^{-4}\Delta^2. \tag{72}$$

In the absence of the fourfold anisotropy the acoustic mode at zero wave vector would have zero energy. This follows from the combined effects of two symmetries. First of all, the diagonal components of the exchange tensor do not contribute to the energy of this mode because these Cu-Nd interactions are completely frustrated. Secondly, as we saw in Eq. (37), the pseudodipolar energy is invariant with respect to rotating the Cu and Nd spins through the same angle, but in an opposite sense. Obviously, introduction of k_4 breaks this symmetry and leads to a nonzero acoustic mode energy.

We can also obtain simple results for wave vectors on the zone boundary, i.e., for $a(q_x+q_y)=\pi$. Along that line $c_y=-c_x$ and the matrices $A(\mathbf{q})$ and $B(\mathbf{q})$ for the Nd sector break up into two identical 2×2 matrices. Neglecting the very small effect of the coupling to the high-energy Cu modes, we thereby find the spin-wave energies to be

$$\omega_\pm^2=(\Delta-4O^+c_x^2\pm M^+)^2-(4O^-c_x^2\mp M^-)^2. \tag{73}$$

It is a good approximation to set $j_z=0$, in which case

$$\omega_\pm^2=\Delta^2-8\Delta O_\perp j_x^2c_x^2\pm2\Delta M_\perp j_x^2. \tag{74}$$

Approximately, therefore, we have two doubly degenerate Nd modes on the zone boundary with energies given by

$$\omega_\pm\approx\Delta-4O_\perp j_x^2c_x^2\pm M_\perp j_x^2. \tag{75}$$

E. Normal modes at arbitrary wave vectors

We have evaluated energies of the normal modes for wave vectors in various high-symmetry directions from Eq. (59). Results for the low-lying (Nd) modes for selected values of the parameters are shown in Fig. 10. We also show the density of spin-wave states for energy up to 0.8 meV.

F. Temperature dependence of normal modes

An approximate treatment of the temperature dependence of the mode energies is based on a generalization of the random-phase approximation. Within this approximation, as developed for spin systems, one replaces S_z (where z is the direction of long-range magnetic order), by its thermally averaged value, $\langle S_z\rangle_T$. For instance, in the relations of Eq. (47a) one replaces S by $\langle S\rangle_T$, for which we use Eq. (1). One sees that S (which we had previously set equal to $\frac{1}{2}$) is now renormalized by a factor $\xi_C(T)\equiv2\langle S\rangle_T$, whereas the transverse components of the Cu spin, which are proportional to $\sqrt{S}$, are renormalized by a factor $\sqrt{\xi_C(T)}$. We follow the same rule for the Nd spin in terms of a factor $\xi_N(T)$ where, neglecting quantum zero-point motion, one has [see Eq. (30)]

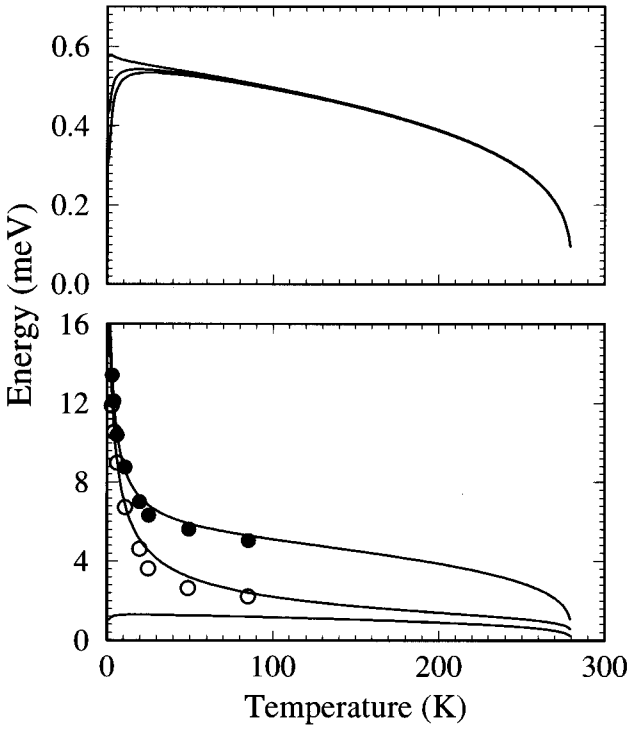

FIG. 11. As in Fig. 10, the full lines are our calculations of the temperature dependence of the spin-wave modes in NCO at zero wave vector. In the top panel we show the three modes at zero wave vector which do not involve motion of the Cu spins. These energies essentially are proportional to the moment of the Cu spins. In the bottom panel we show the three modes at zero wave vector which involve motion of the Cu spins. The experimental points of Ivanov *et al.* (Ref. 17) for two of these modes are shown by filled and open circles. The bottom curve is $200\omega_{ac}$. This mode has not yet been observed.

$$\xi_N(T)=\tanh[\Delta/(2kT)]. \tag{76}$$

Thus the temperature dependence of the spin-wave matrices is obtained from Eqs. (57) and (58) by the replacements

$$H_E\to H_E\xi_C(T),\quad \Delta_C\to\Delta_C\xi_N(T),$$

$$K_n\to K_n[\xi_C(T)\xi_N(T)]^{1/2},$$

$$\Delta\to\Delta_C\xi_C(T)+\Delta_N\xi_N(T)\equiv\Delta(T),\quad X^\pm\to X^\pm\xi_N(T). \tag{77}$$

[Note that where Δ_C appears it actually represents the exchange field acting on the Cu ions due to the Nd moments and hence it is renormalized by a factor $\xi_N(T)$.] In this formulation we treat H_A as a temperature-dependent parameter and although our prescription indicates that $k_4(T)$ is propor-

TABLE IX. Values for the contributions to the splitting in energy of the lowest Nd doublet from various interactions according to mean-field theory. In columns labeled h_N^T we list values (at $T=0$) associated with the interactions $I_n^\perp$ of Thalmeier (Ref. 22) compared to the corresponding values h_J from the interaction J in our theory. The first four columns refer to the exchange field due to Cu spins and the remaining columns to the exchange field due to other Nd spins. Thalmeier's theory has no splitting analogous to ours due to K_{xy} (so we leave the first column of the table blank). Since we have not made any numerical estimates of X and Y, we leave their entries blank. Entries in the last row are all in meV. The total Nd doublet splitting, as defined by Eq. (41), is $\Delta=0.41$ meV using our parameters and 0.44 meV using Thalmeier's.

Cu				Nd							
–	h_K	h_{Cu}	h_Y	h_1	h_M	h_2	h_X	h_3	h_N^T	h_4	h_O
–	$4K_{xy}j_y$	h_{Cu}	$-Y$	$\frac{1}{2}I_1^\perp$	$-2M_\perp j_y^2$	0	$8X$	$-2I_3^\perp$	$8N_\perp j_y^2$	$2I_4^\perp$	$-8O_\perp j_y^2$
–	0.57	0.59		−0.21	−0.18	0		0.14	0.11	−0.08	−0.09

tional to $\Delta(T)$, it may be more realistic to also regard $k_4(T)$ as a temperature-dependent parameter. Following the same analysis as for $T=0$, we now find that the results of Eqs. (62)–(64) become

$$\omega_\pm^2 \approx [\Delta_C\xi_C(T)+\Delta_N\xi_N(T)]^2+2[\Delta_C\xi_C(T) +\Delta_N\xi_N(T)]\xi_N(T)j_x^2[4O_\perp+4N_\perp\pm M_\perp], \quad (78)$$

$$\omega_3^2 \approx [\Delta_C\xi_C(T)+\Delta_N\xi_N(T)]^2+2[\Delta_C\xi_C(T) +\Delta_N\xi_N(T)]\xi_N(T)j_x^2[4O_\perp-4N_\perp-M_\perp], \quad (79)$$

and

$$\omega_4^2 \approx 2H_E\xi_C(T)[H_A+2\Delta_C\xi_N(T)]. \quad (80)$$

The energy of two mixed modes assumes a simple form in the low-temperature limit [when $H_E\xi_N(T)\gg\Delta_C\xi_C(T)$]:

$$\omega_{\mathrm{opt}}^2 \approx 4\Delta_C H_E\xi_N\xi_C, \quad \omega_{\mathrm{ac}}^2 \approx 2k_4(T)[\Delta(T)+2F_z\xi_N(T)], \quad (81)$$

where

$$k_4(T)=\frac{1}{2}\Delta(T)[1-(j_x/j_y)^2]. \quad (82)$$

In the high-temperature limit (when $H_E\xi_N\ll\Delta_C\xi_C$):

$$\omega_{\mathrm{opt}} \approx \Delta_C\xi_C, \quad \omega_{\mathrm{ac}}^2 \approx 8k_4(T)H_E\xi_N(T). \quad (83)$$

In all these results we assumed that (a) H_E dominates all other coupling constants and (b) $\Delta\xi_C(T)\gg k_4(T)$.

The temperature dependence of $\xi_N(T)$ has a very strong effect at temperatures where the thermal energy, kT, passes through Δ. In Fig. 11 we show a graph of the temperature dependence of the modes. In a moment we will discuss the extent to which these results are consistent with experiments.

G. Comparison with experiments

There are several features of our calculations which can be compared with the experimental data. To make this comparison we first discuss how we fix the various parameters which enter the calculation. As mentioned above, the Cu-Cu exchange interactions, which give rise to H_E and H_A are fixed from their values in many other cuprates. In addition, the values of the Nd crystal-field matrix elements, j_x, j_y, and j_z were calculated in Appendix D. We summarize these:

$$H_E=140 \text{ meV}, \quad H_A=0.1 \text{ meV}, \quad (j_x+j_y)/2=1.886,$$

$$j_y-j_x=1.4\times10^{-4}, j_z=-0.015. \quad (84)$$

We note the very small value of j_z. Considering this, the values of the exchange parameters which involve j_z have little influence on the results. Therefore, we have set

$$N_z=M_z=O_z=0. \quad (85)$$

We now fit the other parameters by comparing with the observed spectrum of Nd spin excitations in NCO.[18] In making this comparison we note that the experiment shows more than four low-energy spin-wave modes. This observation indicates that our assumption that the interaction between adjacent three-plane units is negligible, is not totally correct, at least in this context. However, the dispersion along q_z is small, in conformity with our assumption. As a result, the comparison (shown in Fig. 10) of our simple 2D model with the actual data is somewhat approximate. However, we do seem to capture the main physical effects with our simple 2D model. To estimate the numerical values of the parameters, we use Eq. (75) to identify the observed splitting of 0.3 meV at the M point with $2M_\perp j_x^2$, so that

$$2M_\perp j_x^2=0.3 \text{ meV}. \quad (86)$$

Also we note that on average the mode energies are about 0.1 meV higher at the X point ($c_x=c_y=0$) than at the M point ($c_x=-c_y=-1$). Thus we deduce that

$$4O_\perp j_x^2=0.1 \text{ meV}. \quad (87)$$

We now adjust the other parameters, K_{xy} and $N_\perp$ to fit the remaining aspects of the observed spectrum. We found that a reasonable fit to the spin-wave spectrum determined by inelastic neutron scattering[18,19] could be obtained by taking (all in meV)

$$K_{xy}=0.075, \quad K_{xz}=0.01, \quad K_{zz}=0.50, \quad N_\perp=0.004,$$

$$M_\perp=0.025, O_\perp=0.003. \quad (88)$$

Note that with this parameter set, we obtain a reasonable fit to various other data. For instance, in Fig. 11, we show the

temperature dependence of the optical modes involving the Cu sublattices versus temperature. One sees a very good agreement between theory and the observations of Ivanov *et al.*[17] They interpreted their results in a qualitative way as showing two zero wave-vector modes with energy gaps proportional to $\sqrt{H_E H_A}$. The detailed theory presented here gives their argument a firm theoretical basis. Also in Fig. 10 one sees that the density of states indicates a gap to a peak in the density of states at an energy of about 0.28 meV, in spite of the fact that the mean-field splitting Δ given in Eq. (41), is somewhat larger (0.41 meV, see Table IX). This peak value in the density of states is in very good agreement with the detailed analysis of the specific heat of NCO (Ref. 4) which gave a splitting of 0.33 meV (3.7 K in temperature units). Our fit in Fig. 7 to the Nd magnetization in NCO gave 0.30 meV for this splitting. So our theoretical spin-wave spectrum is in broad agreement with the various thermodynamic measurements. Finally, based on our calculations we propose that a measurement of the lowest gap at $q=0$ and low temperatures would be a useful measure of the fourfold anisotropy and would confirm the physics of our model.

H. Comparison with previous calculations

From our results one sees that the approach used by Thalmeier[22] (in which the Cu spins create a fixed exchange field at the Nd sites) is not correct for very small wave vectors. In particular, at zero wave vector such an approach, if used for our model, would give three of the Nd modes correctly, because as we have seen from our exact solution for $\mathbf{q}=0$, these modes are confined to the Nd sublattices. Of course, treating only the Nd spins cannot possibly give a reasonable estimate of the energy of the lowest (acoustic) mode for small q, since this mode is a collective mode of the Nd and Cu sublattices. Our treatment is only necessary near zero wave vector. In fact, from Fig. 10, one sees the extremely strong dependence of the lowest energy mode at small wave vector such that $aq \leqslant \sqrt{\Delta/H_E} \approx 0.06$. For larger q one has four Nd modes with energies near Δ. In treating the acoustic mode it is also important to incorporate the in-plane anisotropy of the Nd doublet, as we have done here. Finally, we give here an approximate treatment of the temperature dependence of the spectrum. Because we assume that the coupling between adjacent three-plane units is small, our calculations apply to all three phases of NCO.

A significant difference between our model and Thalmeier's is that in his work the values assigned to the various exchange tensors are chosen in a way which seems to be inconsistent with the type of order actually found in the various phases. In particular, his choice of the largest Cu-Nd interaction to be a ferromagnetic one (presumably between a Cu spin and the Nd ions directly above and below it in the z direction) seems to be contradicted by the fact that these spins change their relative orientations during the spin reorientation transitions. As discussed in Sec. IV, we would expect that the spin reorientations would preserve the strongest coupling and break only less dominant couplings. This observation motivated our choice of model in which the dominant Nd-Cu interaction is that from the anisotropic exchange interaction between nearest Cu-Nd neighbors. Also, we may mention that the form of the exchange anisotropy in which the Cu-Nd interaction has a tensor with two components, one for interactions in the [001] plane and another for interactions involving z components of spin is not appropriate for the local symmetry of the interaction bond. In fact, as pointed out,[30] the pseudodipolar Nd-Nd interactions arise from the anisotropic exchange interaction only when the correct symmetry of the bond is taken into account. This peculiar symmetry is particularly important in the case of the nearest-neighbor Cu-Nd interactions of Eq. (36). As we have seen, the crucial part of this interaction is the pseudodipolar part proportional to K_{xy}. The other Nd-Nd interactions we use are very similar to those of Thalmeier, as can be seen by the comparison shown in Table IX, where we give the contributions to the splitting from various interactions. [Thalmeier's contribution to the doublet splitting from h_2 (due to his $I_2^{\perp}$) vanishes because he does not allow for the pseudodipolar component of exchange interactions between Nd nearest neighbors.]

Finally we mention the earlier calculation of Sobolev *et al.*[61] In that calculation the degrees of freedom describing the Nd spins have been removed, so that there are just four Cu spins per unit cell. This actually is not too bad, since the highest mode is exact, and the other mode is reasonably close to one of our modes with Nd-Cu mixed in. Of course, this approach cannot describe either the Nd modes or the low-frequency mode due to Nd-Cu collective excitation.

VI. CONCLUSION

We may summarize our conclusions as follows.

(i) We show that due to the exchange field acting on the rare-earth ion and crystalline electric-field interactions, there is a strong single ion anisotropy which aligns the Cu and $R=$Pr, Nd magnetization along the [100] axis, as observed. This same type of calculation also indicates that for Sm in SCO the easy axis lies along [001], again in agreement with observations. Interestingly, our calculation shows that within the plane, the Sm anisotropy favors alignment along [110]. If this anisotropy is the dominant in-plane anisotropy, the magnetic structure would then be a collinear one. The experiments are not conclusive as to whether or not the magnetic structure of SCO is noncollinear, especially in the Sm-ordered phase for $T<6$ K.

(ii) Crystalline electric-field theory with a Cu-R exchange interaction such that the exchange field, defined to couple to $\mathbf{J}$ as in Eq. (2), of the order 0.080 meV for Nd (corresponding to a splitting of the lowest doublet of 0.3 meV), and 0.139 meV for Pr successfully explains many properties, such as the induced R magnetization, the splitting of the Kramers doublet, etc., at all temperatures.

(iii) We propose a model in which a Cu plane with its two Nd neighboring planes form a tightly bound unit due to interactions between the Cu plaquette and the Nd ions adjacent to it. In view of the frustration only pseudodipolar interplanar interactions[21] effectively contribute. We propose a model involving Cu-Cu, Cu-Nd, and Nd-Nd interactions between neighboring tightly bound units. The strengths of the interplanar couplings are assumed to decrease rapidly with distance, but in NCO they can compete because the temperature dependence of the Nd is extremely rapid. This is the simplest model which explains both the three consecutive phase tran-

sitions observed[6] in NCO as well as the absence of such phase transitions in PCO.

(iv) We have calculated the spin-wave spectrum of Nd_2CuO_4 within a simplified three-plane model which qualitatively reproduces the spectrum obtained from inelastic neutron scattering,[18] as is shown in Fig. 10. The resulting Cu-Nd optical modes have a temperature dependence which agrees quite well (see Fig. 11) with the experimental results.[17] The energy of the acoustic spin-wave mode at zero wave vector is predicted to be $\approx\sqrt{2k_4\Delta}\approx 5\mu$eV, where k_4 is the small fourfold anisotropy in the plane and Δ is the splitting of the lowest Nd doublet in the Cu exchange field. This mode has not yet been observed, but clearly its observation is highly desirable.

ACKNOWLEDGMENTS

We acknowledge stimulating interactions with R. J. Birgeneau, A. Boothroyd, M. A. Kastner, J. W. Lynn, and S. Skanthakumar. Work at the University of Pennsylvania was partly supported by the National Science Foundation MRL Program under Grant No. DMR-95-20175 and that at Tel Aviv by the U. S.-Israel Binational Science Foundation, the USIEF, the Israel Science Foundation, and the Sackler Institutes for Theoretical and for Solid State Physics.

APPENDIX A: COEFFICIENTS IN THE PERTURBATION EXPANSION

The coefficients that appear in Eqs. (22) are

$$a_{2i}=\sum_l{}' \frac{x_{il}^2}{E_{i,l}}, \tag{A1a}$$

$$b_{2i}=\sum_l{}' \frac{z_{il}^2}{E_{i,l}}, \tag{A1b}$$

$$a_{3i}=x_{ii}\left(\sum_{l,m}{}' \frac{x_{il}x_{lm}x_{mi}}{E_{i,l}E_{i,m}}-x_{ii}\sum_l{}' \frac{x_{il}^2}{E_{i,l}^2}\right), \tag{A1c}$$

$$b_{3i}=2x_{ii}\left(\sum_{l,m}{}' \frac{x_{il}x_{lm}x_{mi}(\epsilon_{il}-\epsilon_{lm}+\epsilon_{mi})}{E_{i,l}E_{i,m}}-x_{ii}\sum_l{}' \frac{x_{il}^2}{E_{i,l}^2}\right), \tag{A1d}$$

$$c_{3i}=z_{ii}\left(\sum_{l,m}{}' \frac{\Sigma_P(-1)^P P(x_{il}x_{lm}z_{mi})}{E_{i,l}E_{i,m}}-z_{ii}\sum_l{}' \frac{x_{il}^2}{E_{i,l}^2}\right)+x_{ii}\left(\sum_{l,m}{}' \frac{\Sigma_P(-1)^P P(z_{il}z_{lm}x_{mi})}{E_{i,l}E_{i,m}}-x_{ii}\sum_l{}' \frac{z_{il}^2}{E_{i,l}^2}\right), \tag{A1e}$$

$$d_{3i}=z_{ii}\left(\sum_{l,m}{}' \frac{z_{il}z_{lm}z_{mi}}{E_{i,l}E_{i,m}}-z_{ii}\sum_l{}' \frac{z_{il}^2}{E_{i,l}^2}\right), \tag{A1f}$$

$$a_{4i}=\sum_{l,m,n}{}' \frac{x_{il}x_{lm}x_{mn}x_{ni}}{E_{i,l}E_{i,m}E_{i,n}}-\sum_{l,m}{}' \frac{2x_{ii}x_{il}x_{lm}x_{mi}+x_{il}^2x_{im}^2}{E_{i,l}^2E_{i,m}}+x_{ii}^2\sum_l{}' \frac{x_{il}^2}{E_{i,l}^3}, \tag{A1g}$$

$$b_{4i}=2\sum_{l,m,n}{}' \frac{x_{il}x_{lm}x_{mn}x_{ni}(\epsilon_{im}-\epsilon_{il}\epsilon_{mn}+\epsilon_{ln})}{E_{i,l}E_{i,m}E_{i,n}}+2x_{ii}^2\sum_l{}' \frac{x_{il}^2}{E_{i,l}^3}-\sum_{l,m}{}' \frac{4x_{ii}x_{il}x_{lm}x_{mi}(\epsilon_{il}-\epsilon_{lm}+\epsilon_{mi})+2x_{il}^2x_{im}^2}{E_{i,l}^2E_{i,m}}, \tag{A1h}$$

$$c_{4i}=\sum_l{}' \frac{x_{ii}^2z_{il}^2+z_{ii}^2x_{il}^2}{E_{i,l}^3}+\sum_{l,m,n}{}' \frac{\Sigma_P(-1)^P P(x_{il}x_{lm}z_{mn}z_{ni})}{E_{i,l}E_{i,m}E_{i,n}}-\sum_{l,m}{}' \frac{z_{il}^2x_{im}^2+z_{im}^2x_{il}^2}{E_{i,l}^2E_{i,m}}-\sum_{l,m}{}' \left(\frac{2z_{ii}\Sigma_P(-1)^P P(x_{il}x_{lm}z_{mi})}{E_{i,l}^2E_{i,m}}+\frac{2x_{ii}\sum_P(-1)^P P(z_{il}z_{lm}x_{mi})}{E_{i,l}^2E_{i,m}}\right), \tag{A1i}$$

$$d_{4i}=\sum_{l,m,n}{}' \frac{z_{il}z_{lm}z_{mn}z_{ni}}{E_{i,l}E_{i,m}E_{i,n}}-\sum_{l,m}{}' \frac{2z_{ii}z_{il}z_{lm}z_{mi}+z_{il}^2z_{im}^2}{E_{i,l}^2E_{i,m}}+z_{ii}^2\sum_l{}' \frac{z_{il}^2}{E_{i,l}^3}, \tag{A1j}$$

where $E_{i,l}=E_i-E_l$, Σ' indicates that the summed index (or indices) may not assume the value i, and

$$\sum_P(-1)^P P(z_{il}z_{lm}x_{mi})=(z_{il}z_{lm}x_{mi}-z_{il}x_{lm}z_{mi}+x_{il}z_{lm}z_{mi}). \tag{A2}$$

Numerical values of the coefficients are listed in Table VII.

APPENDIX B: COEFFICIENTS OF THE FREE-ENERGY EXPANSION

Here we list the coefficients that appear in the expansions for the free energy and the partition function.

$$\frac{1}{2g_J^2}\chi_\perp = A_Z(T), \tag{B1a}$$

$$\frac{1}{2g_J^2}\chi_z = E_Z(T), \tag{B1b}$$

$$-\alpha_4 = B_Z(T) - \frac{1}{2}\beta A_Z^2(T), \tag{B1c}$$

$$-\beta_4 = F_Z(T) - \frac{1}{2}\beta E_Z^2(T), \tag{B1d}$$

$$-\gamma_4 = C_Z(T) - \beta A_Z^2(T), \tag{B1e}$$

$$-\delta_4 = D_Z(T) - \beta A_Z(T) E_Z(T), \tag{B1f}$$

where

$$\mathcal{Z}(0) = 2\sum_{i=1}^{5} e^{-\beta E_{i0}}, \tag{B2}$$

$$A_Z(T) = 2\mathcal{Z}(0)^{-1}\sum_{i=1}^{5} e^{-\beta E_{i0}}\left(-a_{2i} + \frac{1}{2}\beta x_{ii}^2\right), \tag{B3}$$

$$E_Z(T) = 2\mathcal{Z}(0)^{-1}\sum_{i=1}^{5} e^{-\beta E_{i0}}\left(-b_{2i} + \frac{1}{2}\beta z_{ii}^2\right), \tag{B4}$$

$$B_Z(T) = 2\mathcal{Z}(0)^{-1}\sum_{i=1}^{5} e^{-\beta E_{i0}}\left(-a_{4i} + \frac{1}{2}\beta a_{2i}^2 + \beta a_{3i} - \frac{1}{2}\beta^2 x_{ii}^2 a_{2i} + \frac{\beta^3}{4!}x_{ii}^4\right), \tag{B5}$$

$$C_Z(T) = 2\mathcal{Z}(0)^{-1}\sum_{i=1}^{5} e^{-\beta E_{i0}}\left(-b_{4i} + \beta a_{2i}^2 + \beta b_{3i} - \beta^2 x_{ii}^2 a_{2i} + \frac{2\beta^3}{4!}x_{ii}^4\right), \tag{B6}$$

$$D_Z(T) = 2\mathcal{Z}(0)^{-1}\sum_{i=1}^{5} e^{-\beta E_{i0}}\left(-c_{4i} + \beta a_{2i} b_{2i} + \beta c_{3i} - \frac{1}{2}\beta^2(x_{ii}^2 b_{2i} + z_{ii}^2 a_{2i}) + \frac{2\beta^3}{4!}x_{ii}^2 z_{ii}^2\right), \tag{B7}$$

$$F_Z(T) = 2\mathcal{Z}(0)^{-1}\sum_{i=1}^{5} e^{-\beta E_{i0}}\left(-d_{4i} + \frac{1}{2}\beta b_{2i}^2 + \beta d_{3i} - \frac{1}{2}\beta^2 z_{ii}^2 b_{2i} + \frac{\beta^3}{4!}z_{ii}^4\right). \tag{B8}$$

APPENDIX C: GROUND-STATE ENERGY AND SUSCEPTIBILITY OF PR

We first give the matrix elements involving $\mathbf{h}_\perp$. Here ϕ refers to the angle which $h_\perp$ makes with the x axis:

$$\langle g|\mathbf{J}\cdot\mathbf{h}\begin{pmatrix}|d_1\rangle\\|d_2\rangle\end{pmatrix} = 1.883h_\perp\begin{pmatrix}e^{i\phi}\\-e^{-i\phi}\end{pmatrix};$$

$$\langle g|\mathbf{J}\cdot\mathbf{h}\begin{pmatrix}|D_1\rangle\\|D_2\rangle\end{pmatrix} = 0.675h_\perp\begin{pmatrix}e^{i\phi}\\-e^{-i\phi}\end{pmatrix}, \tag{C1a}$$

$$\langle e_1|\mathbf{J}\cdot\mathbf{h}\begin{pmatrix}|d_1\rangle\\|d_2\rangle\end{pmatrix} = 0.332h_\perp\begin{pmatrix}e^{-i\phi}\\-e^{i\phi}\end{pmatrix};$$

$$\langle e_1|\mathbf{J}\cdot\mathbf{h}\begin{pmatrix}|D_1\rangle\\|D_2\rangle\end{pmatrix} = 1.853h_\perp\begin{pmatrix}e^{-i\phi}\\-e^{i\phi}\end{pmatrix}, \tag{C1b}$$

$$\langle e_2|\mathbf{J}\cdot\mathbf{h}\begin{pmatrix}|d_1\rangle\\|d_2\rangle\end{pmatrix} = 0.876h_\perp\begin{pmatrix}e^{-i\phi}\\e^{i\phi}\end{pmatrix};$$

$$\langle e_2|\mathbf{J}\cdot\mathbf{h}\begin{pmatrix}|D_1\rangle\\|D_2\rangle\end{pmatrix} = 0.483h_\perp\begin{pmatrix}-e^{-i\phi}\\-e^{i\phi}\end{pmatrix}, \tag{C1c}$$

$$\langle e_3|\mathbf{J}\cdot\mathbf{h}\begin{pmatrix}|d_1\rangle\\|d_2\rangle\end{pmatrix} = 1.351h_\perp\begin{pmatrix}e^{-i\phi}\\-e^{i\phi}\end{pmatrix};$$

$$\langle e_3|\mathbf{J}\cdot\mathbf{h}\begin{pmatrix}|D_1\rangle\\|D_2\rangle\end{pmatrix} = 0.797h_\perp\begin{pmatrix}e^{-i\phi}\\-e^{i\phi}\end{pmatrix}, \tag{C1d}$$

$$\langle e_4|\mathbf{J}\cdot\mathbf{h}\begin{pmatrix}|d_1\rangle\\|d_2\rangle\end{pmatrix} = 0.434h_\perp\begin{pmatrix}-e^{i\phi}\\-e^{-i\phi}\end{pmatrix};$$

$$\langle e_4|\mathbf{J}\cdot\mathbf{h}\begin{pmatrix}|D_1\rangle\\|D_2\rangle\end{pmatrix} = 1.953h_\perp\begin{pmatrix}e^{i\phi}\\e^{-i\phi}\end{pmatrix}. \tag{C1e}$$

The only nonzero matrix elements involving h_z are

$$(\langle d_1|\langle d_2|)J_z h_z\begin{pmatrix}|d_1\rangle\\|d_2\rangle\end{pmatrix} = 2.069h_z\begin{pmatrix}1&0\\0&-1\end{pmatrix};$$

$$\langle e_4|J_z h_z|g\rangle = -2.000h_z, \tag{C2a}$$

$$(\langle D_1|\langle D_2|)J_z h_z\begin{pmatrix}|D_1\rangle\\|D_2\rangle\end{pmatrix} = 0.068h_z\begin{pmatrix}-1&0\\0&1\end{pmatrix};$$

$$\langle e_3|J_z h_z|e_2\rangle = 3.190h_z, \tag{C2b}$$

$$(\langle D_1|\langle D_2|)J_z h_z\begin{pmatrix}|d_1\rangle\\|d_2\rangle\end{pmatrix} = 1.692h_z\begin{pmatrix}-1&0\\0&1\end{pmatrix};$$

$$\langle e_2|J_z h_z|e_1\rangle = -2.415 h_z . \tag{C2c}$$

Now we use these results to implement perturbation theory. In our numerical results, all energies and h are expressed in meV. First-order perturbation of the ground state is zero. For the second-order perturbation of the ground state we evaluate terms of the form

$$\sum_{\alpha} \frac{\langle g|V_{\rm ex}|\alpha\rangle\langle\alpha|V_{\rm ex}|g\rangle}{(E_g - E_\alpha)}. \tag{C3}$$

There are two kinds of quantities from this term

$$\sum_{d_1,d_2} \frac{\langle g|V_{\rm ex}|d\rangle\langle d|V_{\rm ex}|g\rangle}{E_g - E_d} + \sum_{D_1,D_2} \frac{\langle g|V_{\rm ex}|D\rangle\langle D|V_{\rm ex}|g\rangle}{E_g - E_D}$$
$$= \frac{2(1.883)^2 h_\perp^2}{E_g - E_d} + \frac{2(0.675)^2 h_\perp^2}{E_g - E_D} = -0.389 h_\perp^2 , \tag{C4}$$

and

$$\frac{\langle g|V_{\rm ex}|e_4\rangle\langle e_4|V_{\rm ex}|g\rangle}{E_g - E_{e_4}} = \frac{-4h_z^2}{98.5} = -0.0406 h_z^2 . \tag{C5}$$

The third-order terms vanish. The fourth-order terms are proportional to $(h_x^4 + h_y^4)$, $h_x^2 h_y^2$, h_z^4 and $h_\perp^2 h_z^2$. There are two types of matrix elements that we have to evaluate:

$$(1) \sum_{\alpha,\beta,\gamma} \frac{\langle g|V_{\rm ex}|\alpha\rangle\langle\alpha|V_{\rm ex}|\beta\rangle\langle\beta|V_{\rm ex}|\gamma\rangle\langle\gamma|V_{\rm ex}|g\rangle}{(E_g - E_\alpha)(E_g - E_\beta)(E_g - E_\gamma)}.$$

From this term we get $-h_\perp^4[9.68\times10^{-4}\cos^2(2\phi) + 3.23\times10^{-4}\sin^2(2\phi)] - 0.00546 h_z^2 h_\perp^2$ which can be written as

$$-9.68\times10^{-4}(h_x^4 + h_y^4) + 6.44\times10^{-4} h_x^2 h_y^2 - 0.00546 h_z^2 h_\perp^2 . \tag{C6}$$

$$(2) -\sum_{\alpha,\beta} \frac{\langle g|V_{\rm ex}|\alpha\rangle\langle\alpha|V_{\rm ex}|g\rangle\langle g|V_{\rm ex}|\beta\rangle\langle\beta|V_{\rm ex}|g\rangle}{(E_g - E_\alpha)(E_g - E_\beta)^2}.$$

This will only give quantities proportional to $h_\perp^4$, h_z^4 and $h_\perp^2 h_z^2$ which are

$$0.00793 h_\perp^4 + 1.674\times10^{-5} h_z^4 + 0.000988 h_z^2 h_\perp^2 . \tag{C7}$$

Hence the ground-state energy in a field is given by

$$E_g = -0.389 h_\perp^2 - 0.0406 h_z^2 + 0.00696(h_x^4 + h_y^4) + 0.0165 h_x^2 h_y^2$$
$$+ 1.674\times10^{-5} h_z^4 - 0.00447 h_\perp^2 h_z^2 . \tag{C8}$$

We also quote here the general formula for the susceptibility for a non-Kramer's ion,

$$\chi_{\alpha\alpha}(T) = \frac{1}{Z}\left\{ \frac{1}{kT}\sum_{\Gamma} e^{-E_\Gamma/kT} \sum_{\Gamma'}{}' |\langle\Gamma|\mu_\alpha|\Gamma'\rangle|^2 \right.$$
$$\left. + \sum_{\Gamma} \sum_{\Gamma'}{}'' |\langle\Gamma|\mu_\alpha|\Gamma'\rangle|^2 \frac{e^{-E_\Gamma/kT} - e^{-E_{\Gamma'}/kT}}{E_{\Gamma'} - E_\Gamma} \right\}, \tag{C9}$$

where μ is the magnetic moment operator, $|\Gamma\rangle$ is a crystal-field state for $h=0$, and E_Γ is the corresponding eigenvalue. Here Σ' indicates a sum over states $|\Gamma'\rangle$ that are identical to or degenerate with $|\Gamma\rangle$, and Σ'' indicates a sum over states $|\Gamma'\rangle$ that are nondegenerate in energy with $|\Gamma\rangle$. The first term gives the temperature-dependence of the magnetic susceptibility and the second term gives a relatively temperature independent paramagnetism.

APPENDIX D: THE STATES $|g\rangle$ AND $|e\rangle$

Here we develop expressions for the states $|g\rangle$ and $|e\rangle$ of the lowest doublet in the presence of an exchange field. For that purpose it is convenient to label the ten zero-field states as doublets from 1 to 5 in order of increasing energy. We use perturbation expansions identical to those of Sec. III.C. to develop expansions for $|g\rangle$ and $|e\rangle$ in terms of the ten doubly degenerate states of the $J=9/2$ multiplet. The exchange field at a Nd ion in an n sublattice due to all its Cu and Nd neighbors lies along the y axis. The magnitude of the exchange field, h, will be fixed to give the observed doublet splitting.

We first diagonalize the potential due to interactions with this magnetic field within the ground-state doublet to give the states $|1\pm\rangle$. We will use the fact, shown in Sec. III C, that the matrix elements of the **J** operators between any two sets of doublets are like Pauli spin matrices. For the n sublattice (with Nd moment along the $-y$ direction) we have

$$\begin{pmatrix} \langle i+| \\ \langle i-| \end{pmatrix} \mathbf{J}(|j+\rangle|j-\rangle) = (x_{ij}\sigma_x, \epsilon_{ij} x_{ij}\sigma_z, -z_{ij}\sigma_y), \tag{D1}$$

where σ are the Pauli spin matrices, i,j are labels of the doublets, and ϵ_{ij}, x_{ij}, and z_{ij} are defined in Eq. (16).

From the diagonalization of the potential matrix (for a field in the $-y$ direction, carried out in Sec. IIIC), we can see that the zeroth-order ground state $|g\rangle_0$ is the state labeled $|1-\rangle$, while the zeroth-order first excited state $|e\rangle_0$ is labeled $|1+\rangle$. Explicitly we have

$$|1-\rangle \equiv |g\rangle_0 = \frac{1}{\sqrt{2}}[|A_1\rangle - i\Theta|A_1\rangle],$$
$$|1+\rangle \equiv |e\rangle_0 = \frac{1}{\sqrt{2}}[\Theta|A_1\rangle - i|A_1\rangle], \tag{D2}$$

where $|A_1\rangle$ and Θ are given in Eqs. (8e) and (9), respectively. At this order there is no difference between the x and y directions, but there is one between the z direction and the x or y directions, reflecting the tetragonal symmetry of the lattice. To see an anisotropy in the $x-y$ plane we need to carry the expansion to higher order. We can find the corrections to the zeroth-order wave function to first ($|1\pm,1\rangle$) second ($|1\pm,2\rangle$) and third order ($|1\pm,3\rangle$) in the fields. These will be orthogonal to the original state, that is, the corrections to any state will only involve the states belonging to the four other doublets. In this formulation the eigenstate is not normalized to unity.

$$|1\pm,1\rangle=\pm\sum_{k=2}^{5} h\frac{\epsilon_{1k}x_{k1}}{E_{1k}}|k\pm\rangle\equiv\pm h\sum_{k=2}^{5}\epsilon_{1k}f_k^{(1)}|k\pm\rangle, \tag{D3a}$$

$$|1\pm,2\rangle=\sum_{k=2}^{5} h^2\epsilon_{1k}\left(\frac{x_{kp}x_{p1}}{E_{1k}E_{1p}}-\frac{x_{k1}x_{11}}{E_{1k}^2}\right)|k\pm\rangle \equiv h^2\sum_{k=2}^{5}\epsilon_{1k}f_k^{(2)}|k\pm\rangle, \tag{D3b}$$

$$|1\pm,3\rangle=\pm\sum_{k=2}^{5} h^3\epsilon_{1k}\left(\frac{x_{kp}x_{pq}x_{q1}}{E_{1k}E_{1p}E_{1q}}-\frac{x_{kp}x_{p1}x_{11}}{E_{1k}E_{1p}^2}-\frac{x_{kp}x_{p1}x_{11}}{E_{1k}^2E_{1p}} +\frac{x_{k1}x_{11}^2}{E_{1k}^3}-\frac{x_{k1}x_{1p}x_{p1}}{E_{1p}E_{1k}^2}\right)|k\pm\rangle \equiv\pm h^3\sum_{k=2}^{5}\epsilon_{1k}f_k^{(3)}|k\pm\rangle, \tag{D3c}$$

where the repeated indices (p,q) are summed from 2 to 5. Let

$$f_k(h)=f_k^{(1)}h+f_k^{(2)}h^2+f_k^{(3)}h^3. \tag{D4}$$

Then the two lowest states are given by

$$|e\rangle=|1,+\rangle+\sum_{k=2}^{5} f_k(h)\epsilon_{1k}|k+\rangle, \tag{D5a}$$

$$|g\rangle=|1,-\rangle+\sum_{k=2}^{5} f_k(-h)\epsilon_{1k}|k-\rangle. \tag{D5b}$$

For the n sublattice (with Nd spin in the $-y$ direction) we have

$$\begin{pmatrix}\langle e|\\ \langle g|\end{pmatrix}\mathbf{J}(|e\rangle|g\rangle)=\left[j_x\sigma_x,\frac{1}{2}(j_{y+}+j_{y-})I +\frac{1}{2}(j_{y+}-j_{y-})\sigma_z,-j_z\sigma_y\right], \tag{D6}$$

where I is the unit 2×2 matrix and the expressions for $j_x\ldots j_z$ are

$$C_eC_gj_x=\langle g|J_x|e\rangle=x_{11}+\sum_{k=2}^{5}\epsilon_{k1}x_{k1}[f_k(h)+f_k(-h)] +\sum_{k,p=2}^{5}\epsilon_{kp}x_{kp}f_k(h)f_p(-h) =\langle e|J_x|g\rangle, \tag{D7}$$

$$C_eC_gj_z=-i\langle g|J_z|e\rangle=\left(z_{11}+\sum_{k=2}^{5} z_{k1}[f_k(h)+f_k(-h)] +\sum_{k,p=2}^{5} z_{kp}f_k(h)f_p(-h)\right) =i\langle e|J_z|g\rangle, \tag{D8}$$

$$C_e^2j_{y+}=\langle e|J_y|e\rangle=x_{11}+\sum_{k=2}^{5} x_{k1}[f_k(h)+f_k(-h)] +\sum_{k,p=2}^{5} x_{kp}f_k(h)f_p(h), \tag{D9}$$

$$C_g^2j_{y-}=C_g\langle g|J_y|g\rangle=-x_{11}-\sum_{k=2}^{5} x_{k1}[f_k(h)+f_k(-h)] -\sum_{k,p=2}^{5} x_{kp}f_k(-h)f_p(-h), \tag{D10}$$

where $C_e^2=\langle e|e\rangle$ and $C_g^2=\langle g|g\rangle$. One sees that $\delta j_y\equiv j_{y+}+j_{y-}$ is of order h^3, and $\delta j_\perp\equiv j_y-j_x$ is of order h^2, where $j_y=(j_{y+}-j_{y-})/2$, whereas j_z and the average in plane $j_{\rm av}\equiv(j_y+j_x)/2$ both are of order h^0. For $\Delta=0.3$ meV, i.e., for $h=\Delta/(2j_y)=0.07954$, we find that $\delta j_y=-1.0\times10^{-6}$, $\delta j_\perp=1.38\times10^{-4}$, $j_z=-0.0151$, and $j_{\rm av}=1.886$.

APPENDIX E: ANISOTROPY DUE TO ZERO-POINT FLUCTUATIONS

In this appendix we consider the effect of the in-plane anisotropy of the Cu-Cu exchange interactions when $\delta J\equiv\mathcal{J}_\parallel-\mathcal{J}_\perp$ is nonzero. We consider only the calculation for $T=0$. Then it is convenient to follow the analysis of Sec. V of Ref. 12. There one sees in Eq. (67) that within noninteracting spin-wave theory there is no gap in the spin-wave spectrum even when δJ is nonzero. Although one can calculate the gap due to δJ using nonlinear spin-wave theory, it is much easier to estimate this gap by constructing an effective Hamiltonian, $\mathcal{H}_{\rm ZP}$, from the dependence of the quantum zero-point energy on the orientation of the staggered moment. This anisotropy is not a long-wavelength phenomenon—in simple cases it can be estimated from the short-wavelength fluctuations.[62,63] Therefore, it is justified to use the effective Hamiltonian given in Eq. (76) of Ref. 12 for the Cu system without any rare-earth spins. In the present notation [and with $J_{\rm av}=(\mathcal{J}_\perp+\mathcal{J}_\parallel)/2$] we have

$$\mathcal{H}_{\rm ZP}=4J_{\rm av}\delta_{\rm in}S^{-3}\sum_{i\in{\rm Cu}} S_{ix}^2S_{iy}^2 =4J_{\rm av}\delta_{\rm in}\left(\sum_{\mathbf{p}}[a_p^2+(a_p^\dagger)^2+2a_p^\dagger a_p] +\sum_{\mathbf{r}}[a_r^2+(a_r^\dagger)^2+2a_r^\dagger a_r]\right), \tag{E1}$$

where $\delta_{\rm in}=2C_2(\delta J/J_{\rm av})^2\approx 10^{-9}$ involves a sum over the zero-point energy of modes in the entire Brillouin zone. This effect is clearly negligible except possibly for zero wave vector. This interaction can be included in the dynamical matrices, in which case in Eq. (60) we should replace H_E by $H_E+4J_{\rm av}\delta_{\rm in}$ and the zero entries in the Cu sector of Eq. (61) should be replaced by $4J_{\rm av}\delta_{\rm in}$. One sees that this modification has no effect at all on the energy of the modes $\omega_{\pm}$ and ω_3, and a completely negligible effect on ω_4. In Eq. (65) we now have the altered matrix elements $A_{11}=H_E+2\Delta_C+4J_{\rm av}\delta_{\rm in}$ and $B_{11}=-H_E+4J_{\rm av}\delta_{\rm in}$. Then, when $\delta_{\rm in}$ can be treated perturbatively, we find

$$\omega_<^2\approx\omega_<^2(\delta_{\rm in}=0)\left(1+\frac{2J_{\rm av}\delta_{\rm in}}{\Delta_c(1-j_x/j_y)}\right). \tag{E2}$$

Using the known values of the parameters we see that including the effect of $\delta_{\rm in}$ has an effect of about 1% on $\omega_<$.

[1] For a review, see J. W. Lynn, in *Physical and Material Properties of High Temperature Superconductors*, edited by S. K. Malik and S. S. Shah (Nova Science, New York, 1994), p. 243.

[2] Y. Tokura, H. Takagi, and S. Uchida, Nature (London) **337**, 345 (1989).

[3] M. Braden, W. Paulus, A. Cousson, P. Vigoureux, G. Heger, A. Goukassov, P. Bourges, and D. Petitgrand, Europhys. Lett. **25**, 625 (1994).

[4] P. Adelmann, R. Ahrens, G. Czjzek, G. Roth, H. Schmidt, and C. Steinleitner, Phys. Rev. B **46**, 3619 (1992). In Eq. (4) of this reference k_BT should be replaced by $2k_BT$. However, the authors apparently used the correct equation in calculating the specific heat, because we did reproduce their Fig. 10(b).

[5] D. Vaknin, S. K. Sinha, D. E. Moncton, D. C. Johnston, J. M. Newsam, C. R. Safinya, and H. E. King , Jr., Phys. Rev. Lett. **58**, 2802 (1987); J. D. Jorgensen, H.-B. Schuttler, D. G. Hinks, D. W. Capone II, K. Zhang, M. B. Brodsky, and D. J. Scalapino, *ibid.* **58**, 1024 (1987).

[6] M. Matsuda, K. Yamada, K. Kakurai, H. Kadowaki, T. R. Thurston, Y. Endoh, Y. Hidaka, R. J. Birgeneau, M. A. Kastner, P. M. Gehring, A. H. Moudden, and G. Shirane, Phys. Rev. B **42**, 10 098 (1990).

[7] I. W. Sumarlin, S. Skanthakumar, J. W. Lynn, J. L. Peng, Z. Y. Li, W. Jiang, and R. L. Greene, Phys. Rev. Lett. **68**, 2228 (1992).

[8] R. J. Birgeneau and G. Shirane, in *Physical Properties of High Temperature Superconductors I*, edited by D. M. Ginsberg (World-Scientific, Singapore, 1989), and references therein.

[9] B. Keimer, A. Aharony, A. Auerbach, R. J. Birgeneau, A. Cassanho, Y. Endoh, R. W. Erwin, M. A. Kastner, and G. Shirane, Phys. Rev. B **45**, 7430 (1992).

[10] V. B. Grande, Hk. Müller-Buschbaum, and M. Schweizer, Z. Anorg. Allg. Chem. **428**, 120 (1977).

[11] T. Thio, T. R. Thurston, N. W. Preyer, P. J. Picone, M. A. Kastner, H. P. Jenssen, D. R. Gabbe, C. Y. Chen, R. J. Birgeneau, and A. Aharony, Phys. Rev. B **38**, 905 (1988).

[12] T. Yildirim, A. B. Harris, A. Aharony, and O. Entin-Wohlman, Phys. Rev. B **52**, 10 239 (1995).

[13] O. Entin-Wohlman, A. B. Harris, and A. Aharony, Phys. Rev. B **53**, 11 661 (1996).

[14] D. Vaknin, S. K. Sinha, C. Stassis, L. L. Miller, and D. C. Johnston, Phys. Rev. B **41**, 1926 (1990).

[15] M. Greven, R. J. Birgeneau, Y. Endoh, M. A. Kastner, B. Keimer, M. Matsuda, and G. Shirane, Phys. Rev. Lett. **72**, 1096 (1994).

[16] S. Skanthakumar, J. W. Lynn, J. L. Peng, and Z. Y. Li, Phys. Rev. B **47**, 6173 (1993).

[17] A. S. Ivanov, P. Bourges, D. Petitgrand, and J. Rossat-Mignod, Physica B **213-214**, 60 (1995).

[18] W. Henggeler, T. Chattopadhyay, P. Thalmeier, P. Vorderwisch, and A. Furrer, Europhys. Lett. **34**, 537 (1996).

[19] H. Casalta, P. Bourges, D. Petitgrand, and A. Ivanov, Solid State Commun. **100**, 683 (1996).

[20] D. A. Yablonsky, Physica C **182**, 105 (1991).

[21] T. Yildirim, A. B. Harris, O. Entin-Wohlman, and A. Aharony, Phys. Rev. Lett. **72**, 3710 (1994).

[22] P. Thalmeier (unpublished).

[23] P. Allenspach, A. Furrer, R. Osborn, and A. D. Taylor, Z. Phys. B **85**, 301 (1991).

[24] A. T. Boothroyd, S. M. Doyle, D. Mc. K. Paul , and R. Osborn, Phys. Rev. B **45**, 10 075 (1992).

[25] Throughout this paper crystallographic directions are referred to the chemical unit cell shown in Fig. 1.

[26] Ph. Bourges, L. Boudarène, and D. Petitgrand, Physica B **180&181**, 128 (1992).

[27] A. B. Harris, Phys. Rev. **132**, 2398 (1963).

[28] S. Chakravarty, B. I. Halperin, and D. R. Nelson, Phys. Rev. B **39**, 2344 (1989).

[29] H. W. de Wijn, R. E. Walstedt, L. R. Walker, and H. J. Guggenheim, Phys. Rev. Lett. **24**, 832 (1970).

[30] T. Yildirim, A. B. Harris, O. Entin-Wohlman, and A. Aharony, Phys. Rev. Lett. **73**, 2919 (1994).

[31] F. C. Chou, A. Aharony, R. J. Birgeneau, O. Entin-Wohlman, M. Greven, A. B. Harris, M. A. Kastner, Y. J. Kim, D. S. Kleinberg, Y. S. Lee, and Q. Zhu, Phys. Rev. Lett. **78**, 535 (1997).

[32] Y. Endoh, M. Matsuda, K. Yamada, K. Kakurai, Y. Hikada, G. Shirane, and R. J. Birgeneau, Phys. Rev. B **40**, 7023 (1989).

[33] I. W. Sumarlin, J. W. Lynn, T. Chattopadhyay, S. N. Barilo, D. I. Zhigunov, and J. L. Peng, Phys. Rev. B **51**, 5824 (1995).

[34] S. Skanthakumar, J. W. Lynn, J. L. Peng, and Z. Y. Li, J. Appl. Phys. **73**, 6326 (1993).

[35] T. Thio and A. Aharony, Phys. Rev. Lett. **73**, 894 (1994).

[36] P. Allenspach, S. W. Cheong, A. Dommann, P. Fischer, Z. Fisk, A. Furrer, H. R. Ott, and B. Rupp, Z. Phys. B **77**, 185 (1989).

[37] G. Shirane, Acta Crystallogr. **12**, 282 (1959).

[38] A. S. Cherny, E. N. Khats'ko, G. Chouteau, J. M. Louis, A. A. Stepanov, P. Wyder, S. N. Barilo, and D. I. Zhigunov, Phys. Rev. B **45**, 12 600 (1992).

[39] J. Akimitsu, H. Sawa, T. Kobayashi, H. Fujiki, and Y. Yamada, J. Phys. Soc. Jpn. **58**, 2646 (1989).

[40] J. W. Lynn, I. W. Sumarlin, S. Skanthakumar, W-H. Li, R. N. Shelton, J. L. Peng, Z. Fisk, and S-W. Cheong, Phys. Rev. B **41**, R2569 (1990).

[41] T. Chattopadhyay and K. Siemensmeyer (unpublished).

[42] D. Petitgrand, L. Boudarène, P. Bourges, and P. Galez, J. Magn. Magn. Mater. **104-107**, 585 (1992).

[43] S. Skanthakumar, Ph. D. thesis, University of Maryland.

[44] P. Dufour, S. Jandl, C. Thomsen, M. Cardona, B. M. Wanklyn, and C. Changkang, Phys. Rev. B **51**, 1053 (1995).
[45] U. Staub, P. Allenspach, A. Furrer, H. R. Ott, S.-W. Cheung, and Z. Fisk, Solid State Commun. **75**, 431 (1990).
[46] S. Katano, R. M. Nicklow, S. Funahashi, N. Mori, T. Kobayashi, and J. Akimitsu, Physica C **215**, 92 (1993).
[47] S. Skanthakumar, J. W. Lynn, J. L. Peng, and Z. Y. Li, J. Magn. Magn. Mater. **519**, 104 (1992).
[48] M. E. Rose, *Elementary Theory of Angular Momentum* (Wiley, New York, 1957).
[49] K. W. H. Stevens, Proc. Phys. Soc. London, Sec. A **65**, 209 (1952).
[50] A. Abragam and B. Bleaney, *Electron Paramagnetic Resonance of Transition Ions* (Clarendon, Oxford, 1970).
[51] A. J. Kassman, J. Chem. Phys. **53**, 4118 (1970).
[52] T. Strach, T. Ruf, M. Cardona, C. T. Lin, S. Jandl, V. Nekvasil, D. I. Zhigunov, S. N. Barilo, and S. V. Shiryaev, Phys. Rev. B **54**, 4276 (1996).
[53] N. W. Ashcroft and N. D. Mermin, *Solid State Physics* (Saunders, Philadelphia, 1976), p. 650.
[54] M. Tinkham, *Group Theory and Quantum Mechanics* (McGraw-Hill, New York, 1964).
[55] K. R. Lea, M. J. M. Leask, and W. P. Wolf, J. Phys. Chem. Solids **23**, 1381 (1994).
[56] S. Jandl, P. Dufour, T. Strach, T. Ruf, M. Cardona, V. Nekvasil, C. Chen, B. M. Wanklyn, and S. Piño, Phys. Rev. B **53**, 8632 (1996).
[57] M. L. Sanjuan and M. A. Laguna, Phys. Rev. B **52**, 13 000 (1996).
[58] T. Yildirim (unpublished).
[59] This form assumes that the x and y axes are parallel to the [100] and [010] axes of the chemical unit cell shown in Fig. 1.
[60] From purely magnetic dipole-dipole interactions one would have $X=-0.74$, $Y=1.00$, and $Z=-0.30$, all in μeV. The algebraic signs of these interactions are such that they tend to destabilize the structure of phase I. They have the wrong sign to explain the jump in the doublet splitting seen by Dufour *et al.* (Ref. 44).
[61] V. L. Sobolev, H. L. Huang, Yu. G. Pashkevich, M. M. Larionev, I. M. Vitebsky, and V. A. Blinkin, Phys. Rev. B **49**, 1170 (1994).
[62] M. W. Long, J. Phys. Condens. Matter **1**, 2857 (1989).
[63] A. B. Harris, in *Disorder in Condensed Matter Physics*, edited by J. Blackman and J. Tagueña (Clarendon, Oxford, 1991).